Examination of photon strength functions for ^{162,164}Dy from radiative capture of resonance neutrons

S. Valenta,[1,*] B. Baramsai,[2,†] T. A. Bredeweg,[3] A. Couture,[3] A. Chyzh,[2] M. Jandel,[3,‡] J. Kroll,[1,§] M. Krtička,[1] G. E. Mitchell,[2] J. M. O'Donnell,[3] G. Rusev,[3] J. L. Ullmann,[3] and C. L. Walker[2,3]

[1]*Institute of Particle and Nuclear Physics, Faculty of Mathematics and Physics, Charles University, CZ-180 00 Prague 8, Czech Republic*

[2]*Department of Physics, North Carolina State University, Raleigh, North Carolina 27695, USA and Triangle Universities Nuclear Laboratory, Durham, North Carolina 27708, USA*

[3]*Los Alamos National Laboratory, P.O. Box 1663, Los Alamos, New Mexico 87545, USA*

(Received 3 August 2017; published 17 November 2017)

The γ rays following radiative neutron capture on ^{161,163}Dy targets were measured with the highly segmented γ-ray calorimeter Detector for Advanced Neutron Capture Experiments at the Los Alamos Neutron Science Center. The γ-ray energy spectra for different multiplicities were gathered for tens of s-wave resonances of both possible spins in each nucleus. Analysis of these spectra within the statistical model enabled us to draw conclusions about dipole photon strength functions with emphasis on the scissors mode. The photon strength functions best describing Dy data are very similar to previously published results on even-even Gd isotopes. It was shown that the scissors mode plays a significant role in the decay of highly excited states up to the neutron separation energy. Measurement of multiple resonances allowed us to assess the fluctuations of experimental spectra and to compare the fluctuations with simulated ones. The size of measured fluctuations is on average smaller than predicted from simulations. However, the results are puzzling as the difference between simulations within the statistical model and experiment is not consistent for both nuclei.

DOI: 10.1103/PhysRevC.96.054315

I. INTRODUCTION

Detailed information about nuclear levels and transitions between them usually exists in a rather restricted range of excitation energy just above the ground state in medium- and heavy-mass nuclei. Properties of the nucleus at higher excitation energies are then described by the statistical model in terms of the level density (LD) and a set of photon strength functions (PSFs) for different transition types. These quantities are necessary for calculations of reaction rates in many different reactions and are important especially in nuclear astrophysics [1,2] and in the development of advanced nuclear reactors [3].

One way to learn about the PSFs and LD is through the spectral analysis of coincident γ rays from neutron capture at isolated neutron resonances, the so-called multistep cascade (MSC) spectra. In this paper, we present results from the analysis of these spectra in well-deformed even-even ^{162,164}Dy isotopes. The spectra from ^{161,163}Dy(n,γ) reaction were measured with the Detector for Advanced Neutron Capture Experiments (DANCE) [4,5]. This highly segmented, highly efficient γ calorimeter is installed at the pulsed neutron beam at the Los Alamos Neutron Science Center (LANSCE) at Los Alamos National Laboratory.

Special interest is paid to the role and properties of the scissors mode (SM). The SM as a concentration of the ground-state $M1$ strength was envisaged from theory [6–8] and discovered in (e,e') measurements [9]. A wealth of information about the SM was gathered in nuclear resonance fluorescence (NRF) experiments [10–14]. In contrast to the NRF experiments, the manifestation of the SM in the decay of excited states, more precisely the character of the SM as a resonance in the magnetic dipole ($M1$) PSF obeying the Brink hypothesis [15], was identified in two-step γ cascade (TSC) experiment [16,17]. This finding was confirmed by charged-particle-induced experiments from the Oslo Cyclotron Laboratory [18–22] and analyses of coincidence spectra from (n,γ) reactions [23–26]. Unfortunately, the strength of the SM in well-deformed even-even nuclei reported from these experimental techniques is not always consistent; see Sec. V C for a detailed discussion. ^{162,164}Dy are the first even-even rare-earth nuclei where data from all three mentioned experimental techniques are available.

In addition, a strong low-energy PSF enhancement—reported before only in lighter nuclei—was recently observed also in heavier nuclei, including rare-earth ones [27], in Oslo-type experiments. A possible influence of this phenomenon was tested as well.

In Sec. II, we describe the experimental technique to measure the γ spectra with the DANCE calorimeter. The modeling of the statistical γ cascades is discussed in Sec. III. Section IV presents information about the PSFs and LD that can be extracted from the measured MSC spectra. A comparison with other available data is given in Sec. V, and consistency of observed fluctuations with predictions of the statistical model is presented in Sec. VI. A summary is provided in Sec. VII.

II. EXPERIMENT

A comprehensive description of the experimental setup and data processing can be found in Refs. [4,5,28,29]. Here we

*valenta@ipnp.troja.mff.cuni.cz

†Present address: Vantage Partners, NASA Glenn Research Center, Brook Park, OH 44142, USA.

‡Present address: Department of Physics and Applied Physics, University of Massachusetts Lowell, Lowell, MA 01854, USA.

§Present address: Institute of Physics, Academy of Sciences of the Czech Republic, Prague, Czech Republic.

TABLE I. Mass and isotopic composition of the measured Dy targets. Also listed are the neutron separation energy S_n of the product nucleus, the range of sum energies used in the data processing (E_Σ), and the critical energy $E_{\rm crit}$ used in simulations.

Target	Mass	Isotope abundance (%)					S_n	E_Σ	$E_{\rm crit}$
	(mg)	^{160}Dy	^{161}Dy	^{162}Dy	^{163}Dy	^{164}Dy	(MeV)	(MeV)	(MeV)
^{161}Dy	31	0.33(2)	95.69(37)	2.52(13)	0.90(8)	0.56(5)	8.197	7.6–8.4	1.87
^{163}Dy	32	0.03(1)	0.36(1)	1.23(2)	96.86(4)	1.52(2)	7.658	7.0–7.8	1.70

restrict ourselves to covering only the basic features and details specific to the Dy capture measurements.

A. Experimental setup

The experiment was performed at the moderated spallation neutron source LANSCE [30], which produces a white spectrum of neutrons with energies ranging from subthermal to hundreds of MeV with a repetition rate of 20 Hz. The neutrons enter the flight path 14 at the Manuel Lujan Jr. Neutron Scattering Center and at 20 m from the spallation target they impinge on the Dy sample located inside the DANCE detector [4,5], an array of 160 BaF_2 scintillation crystals, which covers a solid angle of $\simeq 3.5\pi$. Each crystal serves as a γ spectrometer. A 6-cm-thick ^{6}LiH shell is placed between the sample and the BaF_2 crystals in order to reduce the scattered neutron flux striking the crystals.

In addition to the BaF_2 crystals, the experimental setup includes three other detectors that are used to monitor the neutron flux: a proportional counter filled with BF_3+Ar gas, an n-type surface barrier Si detector, which views a thin ^{6}LiF deposit, and a ^{235}U fission chamber.

Both enriched Dy targets were prepared at the Oak Ridge National Laboratory as self-supporting metal foils with an area $S = 6.45$ cm^2, and their masses and isotopic compositions are specified in Table I. Data were accumulated for one week for each target.

B. Data processing

The DANCE acquisition system [28] is based on digitization of signals from all 160 BaF_2 detectors using four-channel Acqiris DC265 digitizers with a sampling rate of 500 megasamples per second. Intensities of the fast (decay time $\approx$600 ps) and slow (decay time $\approx$600 ns) components of the scintillation signal from each BaF_2 detector are collected independently. The ratio of these two components of the signal is then used for discrimination against the α background from natural radioactivity of Ra in the BaF_2 crystals [5]. A precise time stamp of γ-ray arrival is also stored and all signals are considered to belong to the same event if they arrive within 10 ns.

The energy calibration of the individual DANCE crystals was performed with a combination of γ-ray sources (^{137}Cs, ^{88}Y, ^{22}Na) and the intrinsic radioactivity in the BaF_2 crystals due to ^{226}Ra and its daughters. The latter calibration was conducted on a run-by-run basis to provide the energy alignment of all crystals in the off-line analysis. The detection efficiency of the DANCE detector array for a 1-MeV γ ray is 86% and the total efficiency for detection of a photon from a cascade exceeds 95%. The energy resolution is about 16% and 7% for 1- and 6-MeV γ rays, respectively.

An emitted γ ray does not necessarily deposit its full energy in a single crystal, but rather several, often neighboring, BaF_2 crystals [29]. The number of crystals that fire during γ-ray cascade detection is thus usually higher than the true multiplicity. To bring the detected multiplicity closer to the real one, we combined all contiguous crystals that have fired during an event into *clusters* and considered each cluster as the response of the detector array to a single γ ray. The number of clusters observed in a capture event is called the *cluster multiplicity* M. Although we use the cluster multiplicity, the conclusions presented in this paper do not change regardless of whether the crystal or the cluster multiplicity is used.

Only events corresponding to strong, well-resolved resonances with sufficient statistics and unambiguous spin were analyzed. These resonances were easily identified from the time-of-flight spectrum. A part of this spectrum for ^{161}Dy(n,γ) reaction after its transformation to neutron-energy scale is shown in Fig. 1. Spectra of sums of deposited γ-ray energies, hereafter called *sum-energy spectra*, are for $M = 2$–4 shown in Fig. 2 for a few strong resonances in each isotope. The

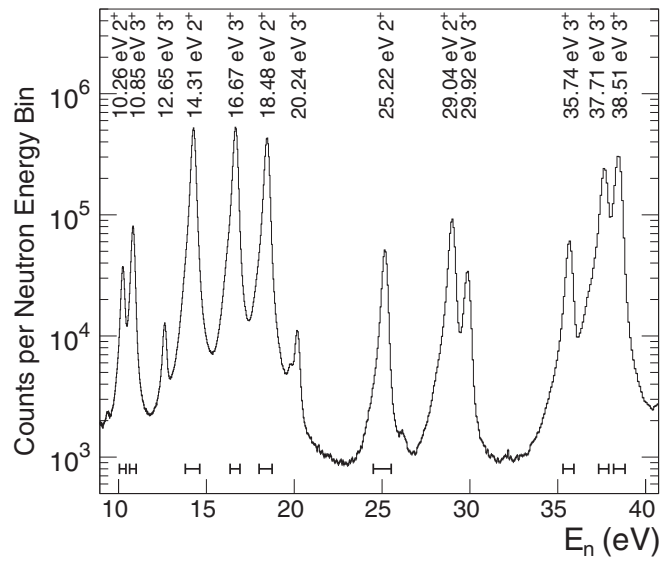

FIG. 1. Time-of-flight spectrum for ^{161}Dy(n,γ) reaction after its transformation to neutron-energy scale. Only events corresponding to multiplicities $M \geqslant 2$ and detected energy sum $E_\Sigma = 7.6$–8.4 MeV were considered. Energies and J^π assignments of resonances are specified. The lines show the ranges of neutron energies used to construct the sum energy and experimental MSC spectra.

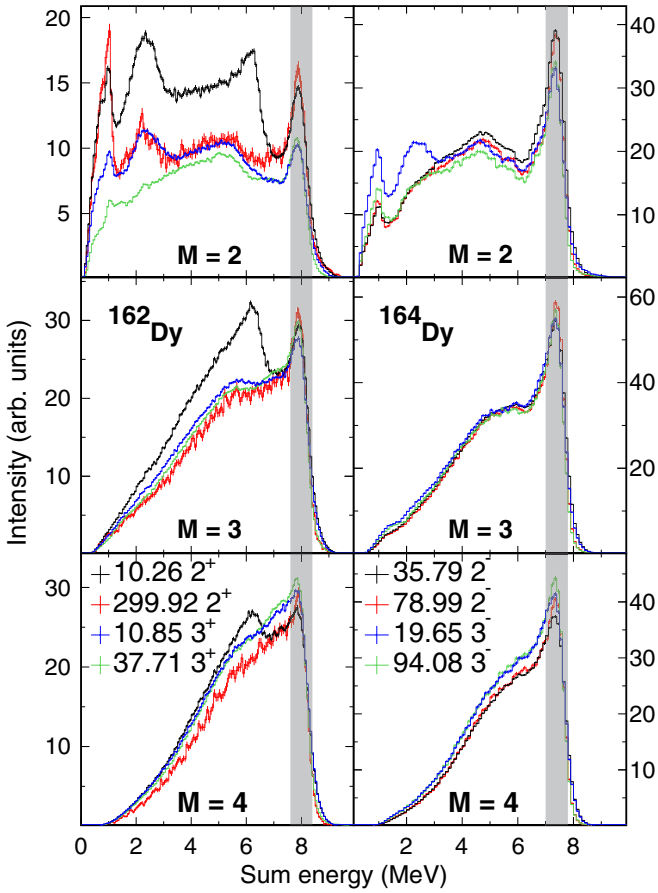

FIG. 2. Examples of sum-energy spectra for individual cluster multiplicities M: left column, ^{162}Dy; right column, ^{164}Dy. Resonance energies and J^π assignments are indicated. The shaded areas represent the E_Σ intervals as specified in Table I. All spectra are normalized as described in Sec. II B. Resonance from ^{160}Dy at 10.45 eV contributes to the sum-energy spectrum of 10.26 eV resonance in ^{161}Dy. The cut on E_Σ eliminates the contribution of the ^{160}Dy resonance to the MSC spectra completely.

spectra are normalized to the same total number of events for $M \geqslant 2$ in the sum-energy range (E_Σ) listed in Table I.

As only s-wave neutron capture plays a role at low neutron energies in this mass region, observed resonances have $J^\pi = 2^+$ or 3^+ in ^{162}Dy and $J^\pi = 2^-$ or 3^- in ^{164}Dy product nuclei. Resonances of different spins have different observed distributions of detected multiplicities M. This fact was exploited to check the spins of resonances in measured nuclei using the method from Ref. [31]. Spins of the majority of strong, well-resolved resonances—which are used in our present analysis—are consistent with values listed in Ref. [32]. A detailed analysis of resonance spins is planned to be published elsewhere.

Each sum-energy spectrum consists of (i) a peak near the neutron separation energy S_n (see Table I), which corresponds to detection of all γ-ray energy emitted in a cascade, and (ii) a low-energy tail, which is formed by events where a part of the emitted γ-ray energy escapes the detection. For low multiplicities, $M < 3$, there is also a strong contribution from background which dominantly comes from natural β radioactivity in the BaF_2 crystals at $E_\Sigma < 3$ MeV. Sometimes resonances in different isotopes have very similar energies to those under study. If there is a strong resonance in an even-mass Dy impurity of the target, a peak at S_n from the product nucleus appears in the spectrum. Such a "parasitic" resonance (from ^{160}Dy target) is clearly visible in the sum-energy spectrum for the 10.26-eV resonance in ^{162}Dy at ≈6 MeV; see Fig. 2.

Events with deposited sum energy falling into regions E_Σ listed in Table I (and depicted as shaded areas in Fig. 2) were used to construct the *experimental MSC spectra*. For a given resonance, an experimental MSC spectrum for multiplicity M was constructed by incrementing counts in M bins corresponding to the γ energies deposited in the M individual clusters within an event. The bin width of 100 keV, which is close to energy resolution of crystals for low energies, was chosen. The experimental MSC spectra inherit the normalization of sum-energy spectra.

The intervals of E_Σ are chosen partly arbitrarily. One of the reasons to use the relatively narrow range of E_Σ when constructing the experimental MSC spectra is to avoid the above-mentioned background contributions. The other reason is that interesting structures observed in the spectra are more pronounced if only cascades depositing all their energies in the detector are considered. Further narrowing of the intervals has minimal impact on the MSC spectral shape and only reduces the statistical precision. Their widening would improve the counting statistics of the experimental MSC spectra but would lead to smearing of the observed structures.

A small background contribution to experimental MSC spectra persists for a given resonance after applying the E_Σ cut. It comes from a contribution of off-resonance capture on target and capture of scattered neutrons in BaF_2 crystals. This contribution can be easily subtracted using experimental MSC spectra from neighboring off-resonance regions on both sides of a resonance.

In total, we obtained experimental MSC spectra for $L_{\rm exp} = 25$ resonances with $J^\pi = 2^+$ and 22 resonances with $J^\pi = 3^+$ from ^{161}Dy(n,γ) reaction and 14 resonances with $J^\pi = 2^-$ and 26 resonances with $J^\pi = 3^-$ from ^{163}Dy(n,γ) reaction. Examples of a few experimental MSC spectra for resonances with both possible spins are plotted in Fig. 3. The spectral shapes are discussed in detail in Sec. IV C.

Uncertainty due to the counting statistics and the background subtraction is usually of the order of a few percent in the midpart of $M = 2$ experimental MSC spectra, for the weakest resonances not exceeding 20%, and even smaller for $M = 3$–6. Spectra for $M = 1$ were not considered in the data analysis as they are often strongly dominated by background. The experimental spectra for $M > 4$ are not shown in the paper as their shape is analogous to $M = 4$ spectra and they do not provide any additional restrictions on the PSFs models apart from reflecting the multiplicity distribution. The multiplicity distribution is in some cases used when discussing acceptability of models in Sec. IV. There are virtually no events with $M > 7$.

To facilitate the comparison of experimental data with model predictions, we constructed the *mean experimental MSC spectra* for each isotope and each group of resonance

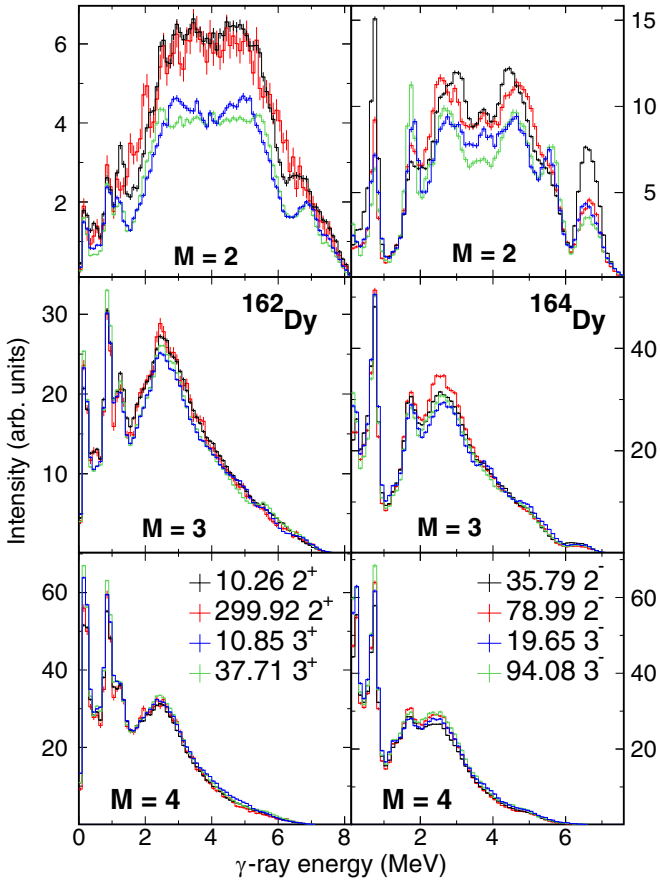

FIG. 3. Examples of experimental MSC spectra for individual cluster multiplicities M: left column, ^{162}Dy; right column, ^{164}Dy. Resonance energies (in eV) and J^{π} assignments are specified. All spectra inherit the normalization as described in Sec. II B.

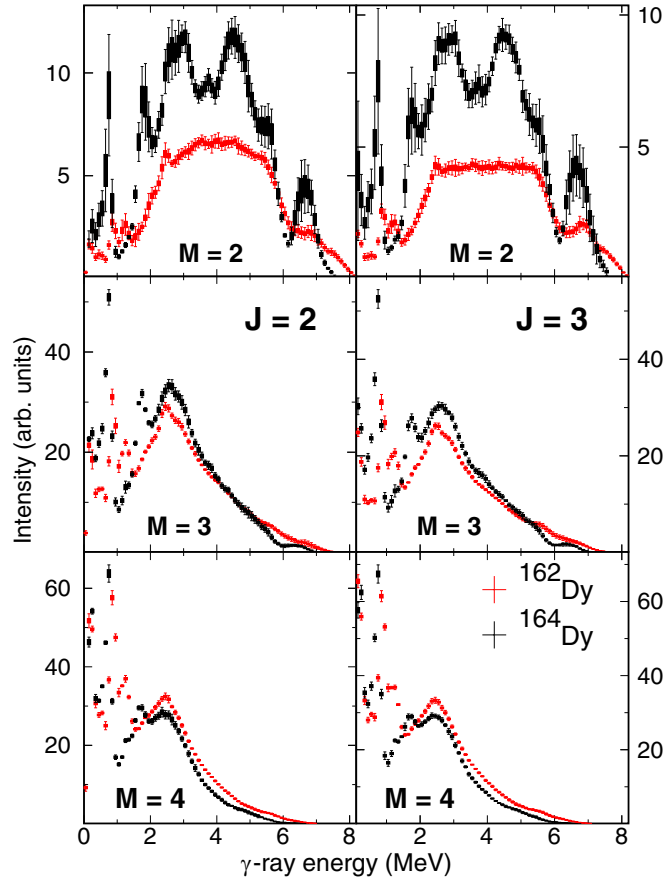

FIG. 4. Mean experimental MSC spectra for individual cluster multiplicities M: left column, $J = 2$ resonances; right column, $J = 3$ resonances. The product isotope is specified. The full rectangles show the mean experimental MSC intensities $I_{\rm exp}$ with their uncertainties coming from the maximum likelihood fit. The error bars represent the width of distribution of experimental MSC intensities, drawn as $I_{\rm exp} \pm \sigma_{\rm exp}$. The spectra inherit the normalization as described in Sec. II B.

spins. For a given bin, we computed the *mean experimental MSC intensity* $I_{\rm exp}$ and the *fluctuation of experimental MSC intensities* $\sigma_{\rm exp}$ using a maximum likelihood fit of the set of experimental MSC intensities and their uncertainties $\{I_\lambda, \Delta_\lambda\}_{\lambda=1}^{L_{\rm exp}}$ of measured individual resonances $\lambda = 1, \ldots, L_{\rm exp}$. The presence of residual fluctuations $\sigma_{\rm exp}$, which is expected due to fluctuations of intensities of primary transitions, is evident from the behavior of the sets $\{I_\lambda, \Delta_\lambda\}_{\lambda=1}^{L_{\rm exp}}$. We assumed that the probability density function describing the distribution of experimental MSC intensities I_λ is a normal distribution. Hence, the likelihood function $\mathcal{L}$ was defined as

$$\mathcal{L} = \prod_{\lambda=1}^{L_{\rm exp}} \frac{1}{\sqrt{2\pi(\sigma_{\rm exp}^2 + \Delta_\lambda^2)}} \exp\left[\frac{-(I_\lambda - I_{\rm exp})^2}{2(\sigma_{\rm exp}^2 + \Delta_\lambda^2)}\right] h(\Delta_\lambda), \quad (1)$$

where $h(\Delta_\lambda)$ is the error distribution.

The resulting mean experimental MSC intensities $I_{\rm exp}$ coincide within uncertainties with the averages of the sets $\{I_\lambda\}_{\lambda=1}^{L_{\rm exp}}$ and have uncertainties of the order of a few percent, not exceeding 10% in any relevant part of spectra. The fluctuations $\sigma_{\rm exp}$ in general reach ≈80% of the standard deviations of the sets $\{I_\lambda\}_{\lambda=1}^{L_{\rm exp}}$; however, they are determined less precisely, typically with 30–80% uncertainty. The mean experimental MSC spectra for $M = 2$–4 are shown in Fig. 4. The uncertainty of $I_{\rm exp}$ as determined from the maximum likelihood fit is displayed as full rectangle in Fig. 4 and Figs. 7–11, while the error bar represents the width of distribution of experimental MSC intensities and is drawn as $I_{\rm exp} \pm \sigma_{\rm exp}$.

III. SIMULATION OF MSC SPECTRA

The experimental MSC spectra, the main observables of our analysis, are products of a complex interplay between the PSFs, LD, and a complicated detector response. As a result, the PSFs and the LD cannot be directly extracted from the experimental MSC spectra. Therefore, we adopted a trial-and-error approach to get information on these quantities—the simulated MSC spectra calculated using various PSFs and LD models are compared with their experimental counterparts. The comparison between the experimental and simulated spectra, as presented in Sec. IV, allowed us to reject many model combinations and choose those most likely to be valid.

A. Algorithms

Utilizing the Monte Carlo DICEBOX algorithm [33], the γ cascades following resonance neutron capture were generated under various assumptions about the LD and PSFs. The response of the DANCE detector, calculated using the Monte Carlo code GEANT4 [29], was subsequently applied to simulated γ cascades.

In the DICEBOX algorithm, below some critical energy, $E_{\rm crit}$, the complete decay scheme is taken from existing experimental data as given in Refs. [34,35] for ^{162}Dy and ^{164}Dy, respectively. The values of $E_{\rm crit}$ (see Table I) were carefully adjusted to ensure that the information about the energies, spins, parities, and decay properties of levels below $E_{\rm crit}$ is complete.

Above $E_{\rm crit}$ up to the capturing state c individual levels and their decay properties are generated using an *a priori* chosen LD function $\rho(E,J,\pi)$ and PSFs $S^{(XL)}$, where X denotes the type (electric, $X \equiv E$, or magnetic, $X \equiv M$) and L is the multipolarity of the transition, $XL = E1$, $M1$, and $E2$. A contribution of higher multipolarities was neglected. A partial radiation width $\Gamma_{i\gamma f}$ for a transition between an initial level i and a final level f is given by

$$\Gamma_{i\gamma f} = \sum_{XL} \frac{\xi_{XL}^2 S^{(XL)}(E_\gamma,T) E_\gamma^{2L+1}}{\rho(E_i,J_i,\pi_i)}, \qquad (2)$$

where ξ_{XL} is a random number drawn from a normal distribution with zero mean and unit variance. This ensures that the individual widths $\Gamma_{i\gamma f}$ fluctuate according to the Porter-Thomas (PT) distribution [36]. $\rho(E_i,J_i,\pi_i)$ is the level density for levels with a given spin J_i and parity π_i at energy E_i of the initial level i. T is the nuclear temperature corresponding to the energy of the final level f, which is a parameter of some of the PSFs models (see Sec. III B). The sum in Eq. (2) goes over all allowed types and multipolarities of transitions, i.e., the mixing of $M1$ and $E2$ is correctly included when permitted. Furthermore, the internal electron conversion plays a noticeable role, especially in the decay of certain low-lying levels. For the transitions above $E_{\rm crit}$ and for those transitions below $E_{\rm crit}$ where the experimental information about internal electron conversion is lacking, DICEBOX computes the contribution of internal electron conversion using parameters from the BrIcc database [37].

Decay branching intensities, $I_{i\to f} = \Gamma_{i\gamma f}/\Gamma_{i\gamma}$, for transitions from any given initial level i below the capturing state c to various final levels f are calculated from a full set of partial radiation widths of given initial level i simulated according to Eq. (2) using the total radiation width of i, $\Gamma_{i\gamma} = \sum_f \Gamma_{i\gamma f}$. Hereafter, the simulated system of all levels below the capturing state c and their branching intensities is referred to as a *nuclear realization* (NR).

In reality, decays of various neutron resonances of the same spin and parity differ only in intensities of primary transitions. To mimic this behavior, we randomly generate the intensities of primary transitions within a given NR. Each set of primary decay branching intensities $I_{c\to f}$ within a given NR is denoted as a *nuclear subrealization*.

Due to the PT fluctuations of partial widths $\Gamma_{c\gamma f}$, there is an enormous number of nuclear subrealizations within a fixed nuclear realization that differ from each other even for fixed PSF and LD models. In addition, for fixed PSF and LD models, there is also an enormous number of nuclear realizations as the levels below the capturing state and their partial widths are generated randomly. Therefore, any simulated observable is subject to inherent, irreducible uncertainties originating from PT fluctuations of the partial radiation widths of randomly generated levels.

Each simulated cascade was processed through a GEANT4 detector response simulation. Different types of information can be obtained from these simulations.

In general, from the simulation of $\lambda = 1,\ldots,L$ nuclear subrealizations within each of $\nu = 1,\ldots,N$ NRs we define, for any given observable $O_{\lambda\nu}$, these measures: (i) a as the mean value, (ii) $a_{\nu'}$ as the mean over nuclear subrealizations within given NR ν', (iii) Σ^2 as the fluctuation of means a_ν over NRs, (iv) $\sigma_{\nu'}^2$ as the fluctuation of $O_{\lambda\nu'}$ over subrealizations in given NR ν', (v) σ^2 as the average of σ_ν^2 over all NRs ν, and (vi) $\Delta_{\lambda\nu}^{\rm MC}$ as the counting uncertainty of $O_{\lambda\nu'}$ due to a finite number of simulated cascades. There are different ways to compute these measures, e.g., simple averaging or maximum likelihood fit on the set $\{O_{\lambda\nu},\Delta_{\lambda\nu}^{\rm MC}\}_{\lambda=1,\nu=1}^{L,N}$.

During the search for appropriate models of PSFs and LD in Sec. IV, we typically simulated $N = 20$ independent NRs with $L = 1$ subrealization for each model combination. Note that in all our previous works, e.g., [23–25], we have always and only used $L = 1$. Usually 10^5 γ cascades were randomly generated for each nuclear subrealization. In this case, the above mentioned quantities are simplified and we compute a as the average value $a = \frac{1}{N}\sum_\nu O_{1\nu}$ and the overall fluctuation as the standard deviation of the set $\{O_{1\nu}\}_{\nu=1}^N$. The observables of interest in this search are mainly the MSC intensities in individual bins of MSC spectra. The simulated ones were constructed in the same way as their experimental counterparts, i.e., if the total deposited energy of simulated γ cascade fell into the E_Σ range from Table I, the event was added to the corresponding simulated MSC spectrum.

Another simulated quantity, which can be compared to its experimental counterpart, is the total radiation width of s-wave neutron resonances Γ_γ. The quantity comes directly from DICEBOX simulations and is discussed in Sec. V B.

In the extended simulations of $N = 50$ NRs with $L = 50$ subrealizations, presented in Sec. VI, the quantities a_ν and σ_ν are computed from the set $\{O_{\lambda\nu},\Delta_{\lambda\nu}^{\rm MC}\}_{\lambda=1}^L$ using a maximum likelihood fit analogously to experimental data processing; see Eq. (1) in Sec. II B. With access to all quantities (i)–(vi) defined above and to fluctuations of experimental MSC intensities $\sigma_{\rm exp}$ we can draw some conclusions not only about the models of PSFs and LD but also about fluctuations of MSC spectra; see Sec. VI.

B. Photon strength functions models

1. Electric-dipole transitions

It is well known that the electric-dipole ($E1$) transitions play a dominant role in the decay of compound nuclei at excitations above the neutron separation energy due to the presence of the giant electric dipole resonance (GEDR). The PSF at these energies in axially deformed nuclei seems to be fully consistent

with the sum of two Lorentzian terms

$$S^{(E1)}_{\mathrm{SLO}}(E_\gamma) = \frac{1}{3(\pi\hbar c)^2}\sum_{i=1}^{2}\frac{\sigma_{G_i}E_\gamma\Gamma^2_{G_i}}{(E^2_\gamma - E^2_{G_i})^2 + E^2_\gamma\Gamma^2_{G_i}}. \quad (3)$$

This model is usually denoted as the Brink-Axel or standard Lorentzian (SLO) model [38]. E_{G_i}, Γ_{G_i}, and σ_{G_i} are the energy, width, and the maximum cross section of the GEDR. We used values of these parameters based on the fit of (γ,xn) experimental data.

Because no (γ,xn) data are available for Dy isotopes, the GEDR parameters from nearby nucleus ^{160}Gd [39] were used. This seems to be fully justified as the GEDR parameters are expected to vary smoothly with A for nuclei with similar deformation. Furthermore, the shape of $S^{(E1)}$ at $E_\gamma \lesssim 9$ MeV, i.e., in the region of our interest, is, within uncertainties of the GEDR parameters, almost indistinguishable when the GEDR parameters are taken from the fit of ^{154}Sm, ^{156}Gd, ^{160}Gd, or ^{168}Er (γ,xn) experimental data [39].

Although there is a common agreement on the $E1$ PSF shape at energies above S_n, the shape of the $E1$ PSF below S_n is not precisely known. Many $E1$ PSF models exist which aim to modify the Lorentzian shape of the low-energy tail of GEDR.

A description of the $E1$ PSF at low E_γ in spherical or weakly deformed nuclei was proposed by Kadmenskii, Markushev, and Furman [40] (KMF model). The model introduced dependence of PSF on nuclear temperature T. Despite the fact that there is no theoretical justification to apply this model in well-deformed nuclei, it is also often adopted.

A modification of the KMF model, in which the T (∼0.3 MeV) is considered to be constant, was used for description of PSFs in Dy isotopes extracted from data on the ^{3}He-induced reaction using the Oslo method [20,21]. Authors of these works argue that for their experimental conditions the excitation energy is relatively low and T is virtually constant in the region of interest. This model, labeled as KMF-T, was found to reasonably reproduce also MSC and TSC spectra of even-even Gd isotopes with $T = 0.3$–0.35 MeV [24,26] and of several odd Gd isotopes with $T = 0.25$–0.40 MeV [25].

Another commonly used model was proposed for spherical nuclei by Chrien [41] in order to match the behavior of the SLO model at energies near the GEDR maxima and that of the KMF model at very low energies. This phenomenological model was later generalized for deformed nuclei [42] by introducing an *ad hoc* parameter k. The systematics of this parameter in Ref. [38] was mainly based on a requirement to reproduce the total radiation widths, Γ_γ. Since Γ_γ strongly depends on the LD below S_n, as well as the PSFs for other transition types, we considered the parameter k to be a free parameter in our simulations. This model is known as the enhanced generalized Lorentzian (EGLO) model. The EGLO model is very similar to the KMF model for $k \sim 1.5$ and strongly enhances low-energy transitions at higher k for decays from highly excited states.

The modified generalized Lorentzian (MGLO) model, introduced in Ref. [25] as an alternative to the EGLO model, makes use of the same parameter k. This model exhibits a significantly smaller preference of low-energy transitions. It was shown that it successfully describes the MSC spectra measured at DANCE in the chain of Gd isotopes [23–25]. The parameter k is considered to be a free parameter in simulations with the MGLO model. For $k \sim 1.5$–2 the $E1$ PSF is rather similar to the KMF model prediction.

In addition, many other models of the $E1$ PSF can be found in the literature. The RIPL-3 database [38]—probably the database most widely used by experimentalists—lists several additional closed-form models. These include the hybrid model (GH) [43], the generalized Fermi liquid (GFL) model [44], and a family of modified Lorentzian (MLO) models [45]. For a comprehensive description of all these models, the reader is referred to Ref. [38]. Further, a PSF model originating from Hartree-Fock-Bogoljubov (HFB) calculations is listed in RIPL-3. All of these models have been tested in our analysis. Many of them use values of E_{G_i}, Γ_{G_i}, and σ_{G_i} as parameters—the same values of these parameters as in the case of the SLO model were adopted.

For a complete description of γ decay, one needs information on the PSFs at all excitation energies. In some models, the dependence on any quantity other than E_γ is neglected. This assumption is known as the Brink hypothesis [15] and was originally formulated for the GEDR $E1$ transitions. Experimental data from average resonance capture [46] and from the ^{3}He-induced reaction [21] do not show any significant deviation from the validity of the hypothesis in the region of excitation energies below S_n. MSC and TSC data are so far inconclusive for $E1$ transitions.

Specifically, from the above-given list of closed-form models, the SLO and KMF-T models are assumed to follow the strict form of the Brink hypothesis. In addition, the hypothesis must be invoked for the description of transitions between excited states in combination with the $E1$ PSF from HFB calculations. All remaining models predict a weak dependence of the PSF on the nuclear temperature T.

The γ-ray energy dependence of the $E1$ PSF for several models is shown in Fig. 5. Two curves of the KMF, MGLO, and MLO models represent how the models change as a function of nuclear temperature – the lower curve corresponds to $T = 0$, i.e., to transitions to the ground state, while the upper one to $T = \sqrt{(S_n - E_\gamma - \Delta)/a_c}$, i.e., to primary transitions. Here, a_c is the LD parameter and Δ is the deuteron pairing energy. The values of a_c and Δ were taken from Refs. [47,48] in conjunction with the corresponding LD model. For the sake of clarity, only a representative sample of the models is drawn in Fig. 5.

The pygmy dipole resonance is observed in several mass regions in the energy range from 6 to 9 MeV [49]. As our data are not very sensitive to this energy range and there is no source of the pygmy dipole resonance parameters in well-deformed rare-earth nuclei, we are not testing for its possible influence. We note that tested $E1$ PSF models might reflect the presence of the pygmy dipole resonance in their shape just below the neutron separation energies of the isotopes studied in this work.

2. *Magnetic-dipole transitions*

The decay of highly excited nuclear states below S_n of deformed rare-earth nuclei is heavily influenced by magnetic dipole ($M1$) transitions. The commonly used models to

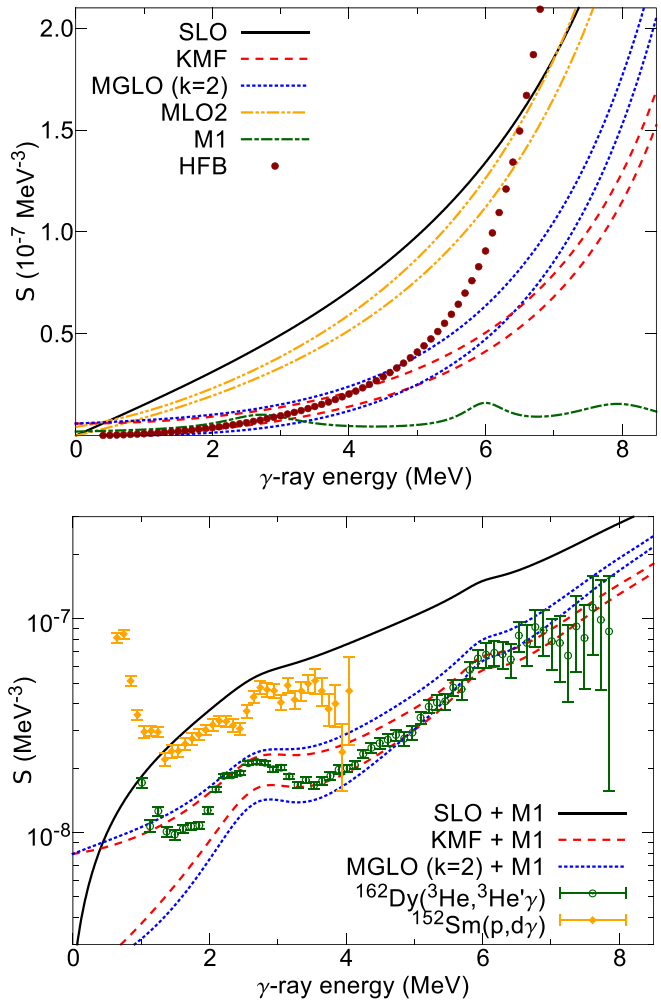

FIG. 5. Photon strength functions as a function of γ-ray energy for some of the models used in our simulations. The upper panel displays the commonly used $E1$ models as well as the $M1$ model consisting of the SM and SF modes and the SP model. The $M1$ PSF parameters are $E_{\rm SM} = 2.8$ MeV, $\Gamma_{\rm SM} = 1.4$ MeV, $\sigma_{\rm SM} = 0.25$ mb, and $S_{\rm SP}^{(M1)} = 2 \times 10^{-9}$ MeV^{-3}. There are two curves for the KMF, MGLO, and MLO2 models of the $E1$ PSF. They indicate how these models change as a function of temperature: The lower curve corresponds to $T = 0$ while the upper one corresponds to $T = \sqrt{(S_n - E_\gamma - \Delta)/a_c}$. The HFB calculation is taken from Ref. [38]. The lower panel shows the sum of $E1$ and $M1$ PSF models from the upper panel as indicated by the labels. The experimental data from ^{3}He-induced and ^{152,4}Sm$(p,d\gamma)$ reactions are from Refs. [20] and [27], respectively.

describe the $M1$ PSF are the single-particle (SP) model, the spin-flip (SF) resonance model, and the scissors mode (SM) model.

In the SP model, the PSF $S_{\rm SP}^{(M1)}$ is a constant independent of γ-ray energy, while in the SF resonance model, the $S_{\rm SF}^{(M1)}(E_\gamma)$ is usually assumed to have a Lorentzian shape with a centroid at about 7 MeV and a width of 4 MeV [38]. Experimentally, the $M1$ strength corresponding to the SF mode was measured for several rare-earth nuclei using inelastic proton scattering [50]. A double-humped structure was observed between 5 and 10 MeV. We adopted a double-resonance Lorentzian parametrization of the SF resonance in our simulations. In our previous MSC and TSC studies [23–26], we successfully represented the $M1$ PSF by a sum of two (SM+SF) models or by the composite $M1$ PSF model as the sum $S^{(M1)} = S_{\rm SM}^{(M1)} + S_{\rm SF}^{(M1)} + S_{\rm SP}^{(M1)}$, which might mimic even more complicated behavior of the $M1$ PSF. The composite $M1$ PSF model was used in the present work unless specified otherwise.

We usually adjusted the absolute value of the $M1$ PSF to reproduce a ratio of $S^{(E1)}/S^{(M1)} \approx 7$ at 7 MeV, observed in several rare-earth nuclei in average resonance capture experiments [46]. If not specifically mentioned, the strict validity of the Brink hypothesis is assumed for all $M1$ models.

In 1976, Hilton [6] and later Iudice and Palumbo [7], using the geometrical two rigid rotor model, and Iachello [8], using the proton-neutron interacting boson model, predicted an isovector $M1$ collective vibrational mode in deformed nuclei: the scissors mode. Experimental observation of the mode for ground-state transitions was made in high-resolution electron inelastic scattering at low momentum transfer in ^{156}Gd [9] and ^{164}Dy [51]; in Dy the $M1$ excitation at 3.1 MeV revealed a transition strength of 1.5(3) μ_N^2.

A systematic study of the mode for the ground-state transitions in rare-earth nuclei was performed with help of the NRF experiments [13,14]. Experimental data indicated that the total observed $M1$ strength in even-even nuclei in the energy range $E_\gamma \approx 2.5$–4.0 MeV is fragmented into several transitions and is proportional to the square of the nuclear deformation [52]. For well-deformed nuclei, the total $M1$ strength reaches $\sum B(M1) \approx 3\ \mu_N^2$ and the centroid of the strength is located near 3 MeV, almost independent of A [53]; in even-even Dy nuclei, the centroids are at 2.870(5), 2.956(4), and 3.143(2) MeV while summed $M1$ strengths in energy range 2.7–3.7 MeV are 2.42(18) μ_N^2, 2.49(13) μ_N^2, and 3.18(15) μ_N^2 for ^{160}Dy, ^{162}Dy, and ^{164}Dy, respectively [10–12].

The experimental PSFs and LDs were obtained for the chain of Dy isotopes from measurements using ^{3}He-induced reactions in Oslo Cyclotron Laboratory [18–22]. The extracted SM was represented by a Lorentzian term in the $M1$ PSF obeying the Brink hypothesis. The determined centroids of the mode are ≈2.65 and 2.81(6) MeV and the total strengths of 6.8(8)μ_n^2 in ^{162}Dy [20] and 5.3(10)μ_n^2 in ^{164}Dy [21], respectively; the width of the Lorentzian curve is ≈1 MeV.

The SM parameters of neighboring nuclei ^{156,158}Gd were extracted from analysis of MSCs from resonance neutron capture. Experimental data allow for a SM position of 2.7–3.1 MeV in ^{156}Gd [24] and 2.8–3.1 MeV in ^{158}Gd [23]. The width of the mode is ≈1 MeV, while the allowed total SM strengths are comparable to the NRF data and 2–3× lower compared to the Dy Oslo results, specifically 1.9–3.5μ_n^2 in ^{156}Gd [24] and 1.4–2.8μ_n^2 in ^{158}Gd [23]. The TSC data from thermal neutron capture in the same Gd isotopes [26] were found to be less sensitive to the parameters of SM, allowing wider yet compatible intervals. Data from both MSC and TSC experiments were fully compatible with the SM represented by a single-Lorentzian term following the Brink hypothesis.

Recently, the PSF extracted from the measurement of ^{152,154}Sm$(p,d\gamma)$ reactions with Ge clover detectors using the Oslo method revealed a strong low-energy PSF enhancement [27]. Similar, albeit stronger, enhancement was reported earlier in lighter nuclei. The shell model calculations for lighter nuclei [54–57] indicate the $M1$ nature of a low-energy enhancement with the exponentially decreasing dependence on the γ-ray energy. In particular, Sieja [57] calculated both the $E1$ and the $M1$ PSFs in lighter nuclei resulting in the $M1$ low-energy PSF enhancement and a flat, nonzero $E1$ PSF for $E_\gamma \to 0$. The analysis of the $M1$ strength in Ref. [56] shows that the sum of the low-energy PSF enhancement and the SM strength does not significantly vary throughout the chain of Fe isotopes. While these calculations deal with lighter nuclei, authors of Ref. [55] argue that the $M1$ low-energy enhancement is expected in nuclei throughout the nuclear chart. There are also calculations suggesting the $E1$ character of the low-energy enhancement, e.g., Ref. [58]. We made several tests of a possible influence of the low-energy enhancement on the decay of ^{162,164}Dy. The $M1$ as well as the $E1$ character of the enhancement following the Brink hypothesis was checked. For details, see Sec. IV C.

3. *Electric-quadrupole transitions*

In addition to dipole transitions, electric quadrupole ($E2$) transitions might also play a role in the cascade decay of neutron resonances. If $E2$ transitions are not extremely strong, any effect of them is similar to that of $M1$ transitions due to the same parity selection rules. The use of the giant quadrupole resonance model is recommended in Ref. [38]. Nonetheless, we adopted a simple single-particle model ($S_{SP}^{(E2)} = \text{constant}$) in the majority of our simulations. $S_{SP}^{(E2)}$ was adjusted to reproduce the ratio of partial radiation widths at about 7 MeV measured in average resonance capture experiments in deformed nuclei ($\Gamma(E1)/\Gamma(E2) \gtrsim 100$) [46]. Under these conditions, our results do not depend on the choice of the $E2$ PSF model.

C. Level density models

There are many models and calculations of LD available in the literature. We tested two different models for the energy dependence of the LD given by closed-form formulas: (i) the back-shifted Fermi gas (BSFG) and (ii) the constant-temperature (CT) model [47]. There are two adjustable parameters in each of these models. Two different parameter sets were tested for each of these LD models [47,48]. The spin dependence of the LD was adopted in the standard form [59], with the spin-cutoff parameter given by corresponding parametrizations from Refs. [47,48].

The effect of even-odd spin staggering in the spin distribution [60–62] was tested in a few simulations and found to have no or little impact on the results. In these tests, the staggering of Ref. [48] was assumed to linearly decrease with excitation energy and to disappear at 3.9 MeV in agreement with shell model Monte Carlo (SMMC) calculations [63]. The parity dependence of the LD was neglected in the majority of simulations above E_{crit}. However, the influence of possible parity dependence was also tested using the formula from Ref. [64]—parameters of the formula were adjusted to reproduce the SMMC calculation [63], where the parity asymmetry disappears near $E = 3$ MeV.

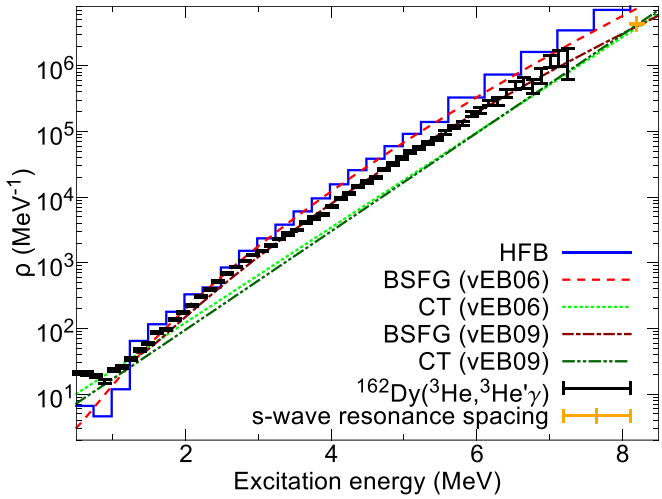

FIG. 6. Spin- and parity-summed level density for ^{162}Dy according to the CT and BSFG models and the HFB calculations. The parameters of the CT and BSFG LDs were taken from Refs. [47] and [48], denoted as (vEB06) and (vEB09) respectively. The experimental data from the Oslo method [18] are also shown. Different predicted absolute values at $S_n = 8.197$ MeV originate from different spin distributions in the models. The point corresponding to the s-wave resonance spacing [32] was converted to the summed LD using the spin distribution with the spin-cutoff parameter from Ref. [48].

From the "microscopic" calculations of LD, we considered two in particular. The authors of Refs. [38,65,66] used Hartree-Fock-Bogoljubov (HFB) plus a combinatorial method to obtain the tabulated LD as a function of energy for levels with each spin and parity, hereafter denoted as HFB LD. These calculated level densities usually suffer from difficulties in reproducing the cumulative number of observed low-lying levels as well as the average neutron resonance spacing. In order to bring the calculations into agreement with experimental data, the HFB LD was suggested to be renormalized [65]. We used the renormalized version. The HFB LD exhibits a much wider spin distribution than all above-discussed models with persisting even-odd spin staggering at practically all excitation energies below S_n. The excess of positive-parity levels in this model is seen up to about 4 MeV.

The energy dependence of LD SMMC calculation in ^{162}Dy by Alhassid *et al.* [63] is claimed to be compatible with the BSFG formula from Ref. [62] between E_{crit} and S_n. As a result, the simulations using this calculation with the above mentioned SMMC spin and parity dependence of LD are practically identical to simulations with the BSFG model [48].

The spin- and parity-summed LD, given by the above-mentioned models, in ^{162}Dy is shown in Fig. 6 together with data from ^{162}Dy(^{3}He,^{3}He$'\gamma$) reaction [20]. The energy dependence of the Oslo experimental data was reproduced by the BSFG model [48] in our analysis.

IV. RESULTS

Almost all possible combinations of PSF and LD models introduced in Secs. III B and III C were tested in simulations and compared with the experimental spectra. A search for the appropriate $M1$ PSF was performed by sampling the SM and SP parameters within reasonable ranges. Altogether, several thousands of individual simulations were computed.

To quantify the degree of agreement between the simulated and experimental MSC spectra, enormously time-consuming simulations with extremely large number of NRs would be needed as the contents of individual bins in MSC spectra are mutually correlated in a complicated fashion and the corresponding correlation matrix is *a priori* not known. As a consequence, within the search for suitable PSF and LD models, the degree of agreement was checked only visually.

As mentioned in Sec. III A we simulated $N = 20$ NRs with $L = 1$ subrealization for each PSF and LD model combination. As will become evident from the discussion in Sec. VI, use of simulations with $L = 1$ turns out to be well justified for simple search of appropriate PSF and LD models.

The results of simulations, plotted as a gray band, are compared in Figs. 7–11 with the mean experimental MSC spectra. The gray band is centered at the average of the set of simulated MSC intensities $\{I_{1\nu}\}_{\nu=1}^{N}$ and has a width of two standard deviations of the set. These fluctuation corridors from simulations should be, in general, broader than those for experimental spectra—the experimental ones rather correspond to the fluctuations obtained from simulations of different subrealizations. However, results on fluctuation properties discussed in Sec. VI indicate that the difference in the width of fluctuation corridors from various subrealizations and from simulations checked in this section should be rather small for the majority of bins.

We should stress that within the enormous domain of PSFs and LD functions the adopted trial-and-error method does not guarantee finding a fully correct model combination. Nevertheless, we did find several combinations of PSF and LD models which lead to a reasonable reproduction of the experimental MSC spectra; see below. As the influence of the $E2$ PSF on the shape of simulated MSC spectra is negligible, we restrict our discussion only to the LD, $E1$, and $M1$ PSFs.

A. Level density

From LD models introduced in Sec. III C, the best description of experimental MSC spectra was obtained using the BSFG model. The older parametrization [47] yields a good agreement for both isotopes. Employing the newer parametrization [48] with even-odd spin staggering and parity asymmetry described in accord with SMMC calculations [63] does not significantly change the results but some differences are observed in higher ($M \geqslant 3$) multiplicities.

The CT model, when used in either isotope, has huge difficulties to simultaneously reproduce intensities in $M = 2$ spectra for both capturing spins with the same PSF models. Furthermore, in ^{164}Dy we failed to reproduce the multiplicity distribution with any tested PSF model combination. Despite the fact that we cannot definitely reject the validity of the CT model as we tested only a finite number of PSF models, our findings together with low predicted values of the total radiation width with the CT model (see Sec. V B) strongly indicate that this LD model is inadequate for even-even Dy isotopes.

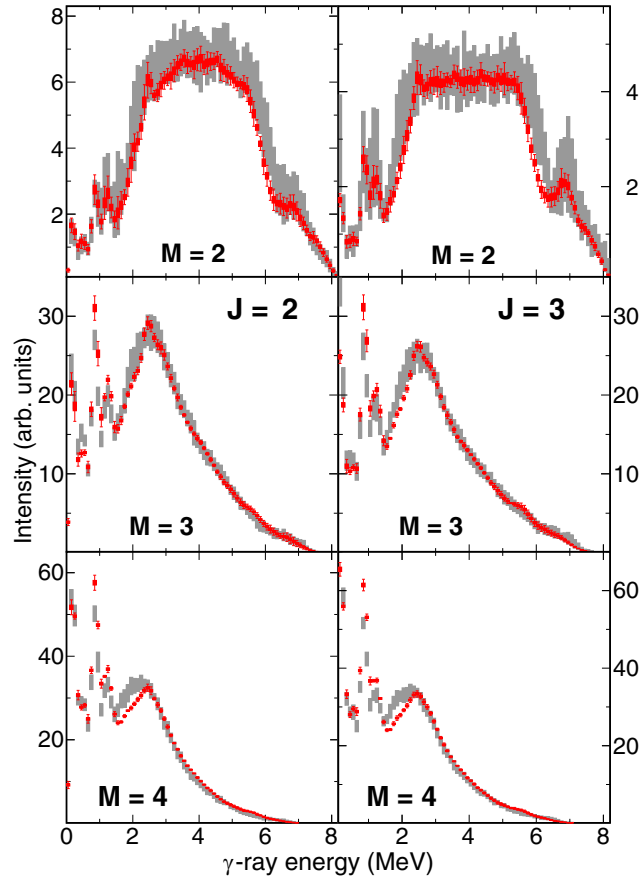

FIG. 7. Comparison of ^{162}Dy mean experimental MSC spectra with simulations using the MGLO $E1$ PSF model and the composite $M1$ PSF model. The k, SM, and SP parameters were adjusted to best describe the mean experimental MSC spectra. The full red rectangles show the mean experimental MSC intensities $I_{\rm exp}$ with their uncertainties coming from the maximum likelihood fit. The red error bars represent the width of distribution of experimental MSC intensities, drawn as $I_{\rm exp} \pm \sigma_{\rm exp}$; see Sec. II B. The gray band corresponds to the result of simulations drawn as a two standard deviation corridor centered at the average MSC intensity; for details, see Sec. III A.

Problems with reproduction of multiplicity distribution also appears for the HFB LD calculation [65]. In this case, the simulations give a high average multiplicity, very likely as a result of significantly higher fraction of levels with high spins in this LD calculation.

B. Electric dipole PSF

All $E1$ PSF models introduced in Sec. III B were tested with the $M1$ strength parameters adjusted separately for each model. We were able to reasonably reproduce experimental MSC spectra for both isotopes when using the KMF, KMF-T

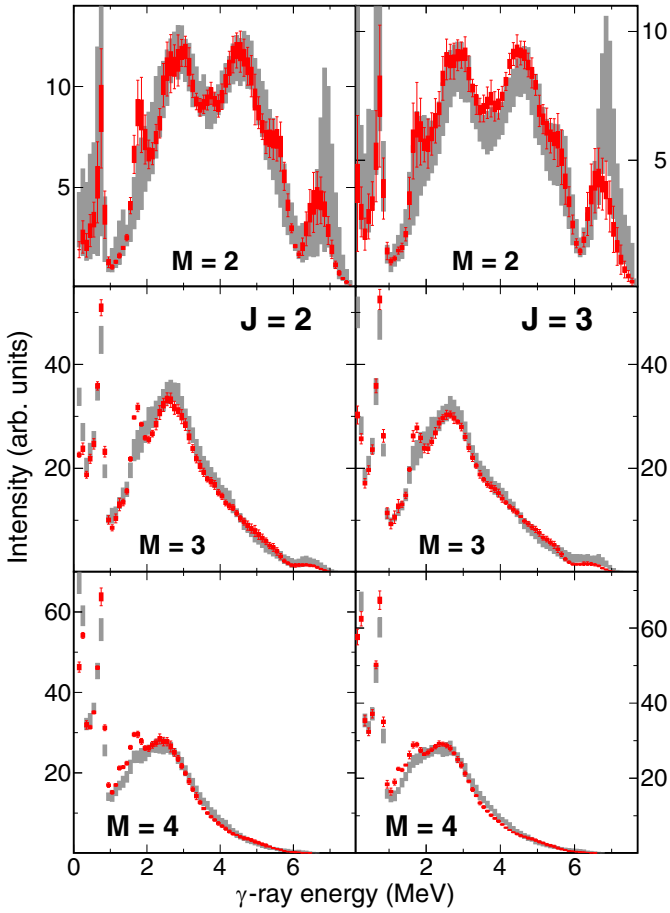

FIG. 8. Comparison of ^{164}Dy mean experimental MSC spectra with simulations using MGLO $E1$ PSF model and the composite $M1$ PSF model. The k, SM, and SP parameters were adjusted to best describe the mean experimental MSC spectra. For additional details, see Fig. 7.

(with $T \approx 0.3$ MeV), GH, and MGLO models; see examples with the MGLO model in Figs. 7 and 8. The simultaneous success of the KMF and GH models is expected as their shapes are very similar in the energy region $E_\gamma \leqslant S_n$. In case of the MGLO model, the value of k parameter to be used is between about 2 and 4 for ^{162}Dy and between about 2 and 5 for ^{164}Dy. The value of the k parameter can be further restricted by the total radiation width; see Sec. V B.

No simulation performed with the rest of the $E1$ PSF models, namely the SLO, EGLO, GFL, and MLO models and the HFB calculation, is able to reproduce experimental MSC spectra of either isotope. Every $S^{(E1)}$ model that shows an increase with E_γ similar to the SLO model at $E_\gamma \lesssim 5$–6 MeV generates more transitions with higher energies. This leads to a multiplicity distribution shifted to smaller values than observed experimentally. We can conclude that $E1$ PSF (at least for transitions between excited states) is relatively flat at relevant γ energies. We should note that there is only a limited number of primary transitions to levels at very low excitation energies, which makes the analysis almost insensitive to $E_\gamma \gtrsim 6$–7 MeV.

A reasonable description of the MSC spectra was achieved also with the KMF-T model with T restricted to be between about 0.30 and 0.35 MeV. This result indicates that the question whether the $E1$ PSF depends on excitation energy for energies at the low-energy tail of GEDR cannot be unambiguously answered from the present study of resonant neutron capture.

C. Magnetic dipole PSF

The presence of a resonance in the $M1$ PSF at energy just below 3 MeV can be deduced by inspection of experimental MSC spectra without the need for simulations.

The experimental MSC spectra of multiplicity $M = 2$ exhibit considerably different shapes in the two isotopes; see Fig. 4. The spectra in ^{162}Dy display a rather flat midpart between energies $E_\gamma \approx 2.5$–5.5 MeV, while in ^{164}Dy there are two distinct bumps at $E_\gamma \approx 2.8$ and 4.5 MeV for spectra of both possible spins of capturing states.

If we assume that the dipole transitions dominate the decay, then the difference of spectral shapes likely reflects the different composition of the cascades. Because of the opposite parity of neutron resonances of the studied nuclei and the E_Σ cut selecting the cascades which terminate at the levels of the ground-state rotational band, the $M = 2$ spectra are almost exclusively formed by $E1$-$E1$ and $M1$-$M1$ cascades in ^{162}Dy while by $E1$-$M1$ and $M1$-$E1$ cascades in ^{164}Dy.

The bumps in ^{164}Dy $M = 2$ spectra and the flatness of those spectra of ^{162}Dy point to the presence of $M1$ resonance at $E_{SM} \approx 2.8$ MeV. The absence of the bumps in the ^{162}Dy $M = 2$ spectra reflects the fact that the position of the resonance energetically forbids two-step $M1$ cascades from reaching the low-lying levels.

The $M1$ character of the resonance seems to be also nicely compatible with the shape of $M = 3$ spectra—the bump just below 3 MeV in ^{162}Dy is rather strong (compared to other multiplicities), indicating a strong contribution of the $M1$-$M1$-$M1$ cascades, while a bump near 1.8 MeV in ^{164}Dy perfectly corresponds to the picture of the strong $M1$-$M1$-$E1$ cascades through the negative-parity levels near the excitation energy of 1.8 MeV, that is, via states at excitation energy $S_n - 2 \times E_{SM}$.

Indeed, simulations without any resonance near 3 MeV in the PSFs yield unacceptable results for all $E1$ models introduced in Sec. III B. In particular, using combinations of the $E1$ and the $M1$ PSF models as recommended in RIPL [38] yield unsatisfactory description of the mean experimental MSC spectra. The change of simulations induced by removing the SM from the $M1$ PSF used in Fig. 7 is shown in Fig. 9.

We have also confirmed that this resonance structure cannot be of $E1$ type. See Fig. 10 showing simulations for ^{164}Dy. Convincing disagreement is also achieved for ^{162}Dy. The possibility to reproduce the mean experimental MSC spectra with the resonance in the $E2$ PSF was tested as well. The discrepancies are smaller than in the case of the $E1$ resonance. Nevertheless, the $M1$ character is favored. We identify the $M1$ resonance as the scissors mode.

Assuming that the SM consists of a single-Lorentzian term [see Eq. (3)], we found that the mean experimental MSC spectra are rather sensitive to the resonance parameters.

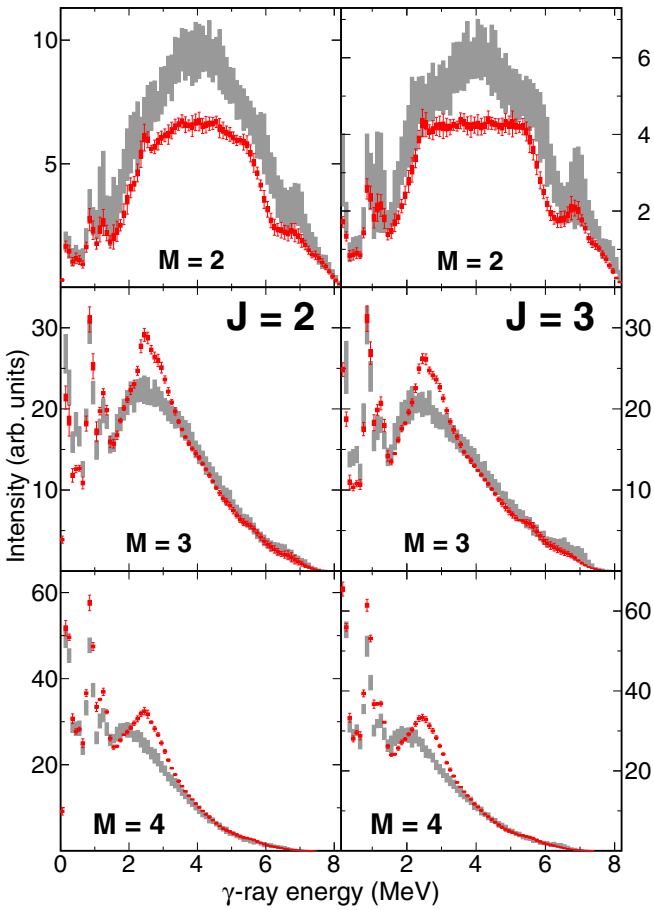

FIG. 9. Comparison of ^{162}Dy mean experimental MSC spectra with simulations without any resonance structure near 3 MeV. The MGLO $E1$ PSF model and the SP+SF models of $M1$ PSF were used with parameters identical to those of simulations in Fig. 7. For additional details, see Fig. 7.

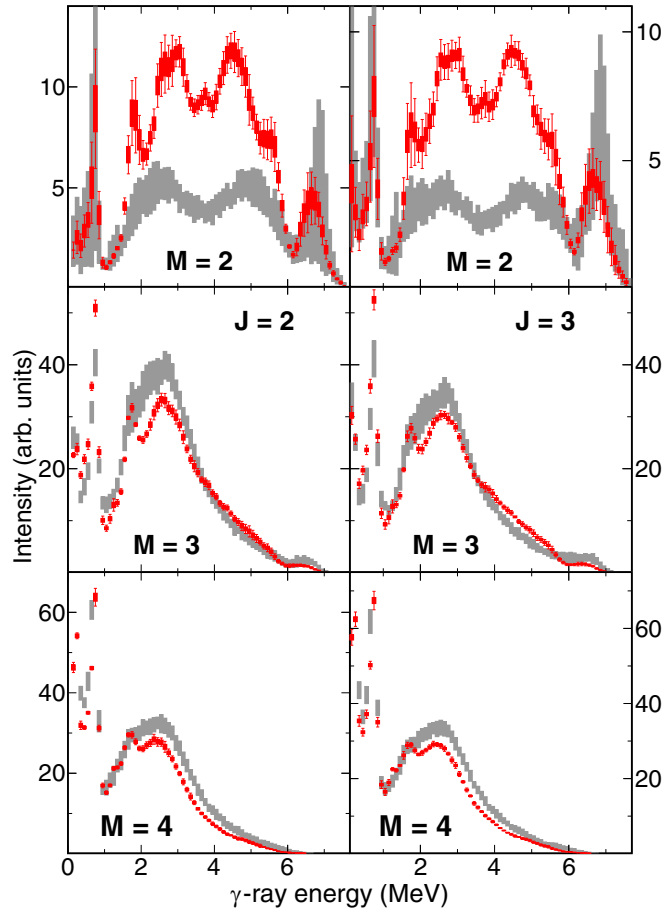

FIG. 10. Comparison of ^{164}Dy mean experimental MSC spectra with simulations having a resonance near 3 MeV in $E1$ PSF. This resonance in the SLO form was added to the MGLO $E1$ PSF model with the $M1$ PSF containing the SF resonance. For additional details, see Fig. 7.

The common result for both isotopes is that the acceptable description of experiment was found for simulations with the SM position $E_{\mathrm{SM}} = 2.8$–3.0 MeV and the damping width of the scissors mode $\Gamma_{\mathrm{SM}} = 1.0$–$1.4$ MeV. This result is almost independent of the choice of the accepted $E1$ PSF models.

On the other hand, the optimal value of the maximum cross section of the scissors mode, σ_{SM}, is strongly correlated with a choice of the $E1$ PSF model and its parameters: As the value of $S^{(E1)}$ is higher, the σ_{SM} becomes stronger. We found that acceptable values of σ_{SM} range from about 0.2 mb for KMF and MGLO ($k = 2$) models to about 0.6 mb for MGLO ($k = 4$). We should mention that the allowed value of σ_{SM} is coupled to values of E_{SM} and Γ_{SM} as well.

We also performed some tests related to possible violation of the Brink hypothesis for the SM. We performed a simple test where the mode is built only on states below certain excitation energy E_{tr} and vanished completely above this excitation energy. Sizable discrepancies between experiment and predictions were observed up to $E_{\mathrm{tr}} \approx 5.5$ MeV in both nuclei. Although we cannot guarantee the exact validity of the Brink hypothesis for the SM, the data indicates that the SM plays a role in primary transitions in agreement with findings on neighboring Gd nuclei [23–26].

In order to achieve a satisfactory agreement of simulations with the ^{162}Dy experimental data, comparable to that shown in Fig. 7, it is necessary to combine the SM and SF also with the SP model. The optimal $S_{\mathrm{SP}}^{(M1)}$ value again depends on the absolute values of the SM and $E1$ PSF: $S_{\mathrm{SP}}^{(M1)} = 2$–$4 \times 10^{-9}$ MeV^{-3} is required in combination with the KMF and MGLO ($k = 2$) models while $S_{\mathrm{SP}}^{(M1)} \approx 8 \times 10^{-9}$ MeV^{-3} with the MGLO ($k = 4$). We should stress that the SP part of the $M1$ PSF is crucial for reproduction of experimental spectra. The simulations without the SP model predict correct shapes of the spectra but clearly underestimate intensities in $M = 2$ spectra and overestimate intensities in $M \geqslant 4$ spectra.

On the other hand, the best descriptions of ^{164}Dy mean experimental MSC spectra were found without using the single-particle model. Within the sensitivity of our data, we cannot completely rule out the presence of a weak SP part in $M1$ PSF, but its strength has to be $S_{\mathrm{SP}}^{(M1)} < 1 \times 10^{-9}$ MeV^{-3} for all model combinations which are able to describe the experimental data in this nucleus.

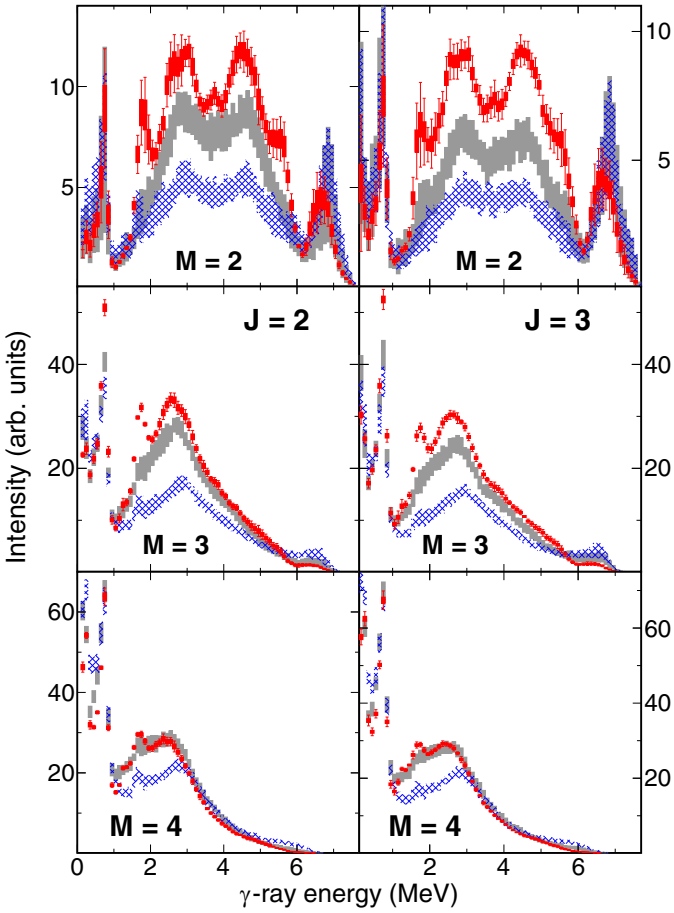

FIG. 11. Comparison of the mean experimental MSC spectra of ^{164}Dy with simulations (i) (blue hatched bands) using the PSF models, including the $M1$ low-energy enhancement in the exponential form, deduced in Ref. [27] and scaled down to the Oslo data [21], (ii) (gray full bands) utilizing a low-energy resonance based on the data from the ^{152,4}Sm$(p,d\gamma)$ experiment [27]. The parameters of the low-energy resonance are specified in the text of Sec. IV C. The GLO model for the $E1$ PSF and the SM+SF resonances for the $M1$ PSF were used in accordance with Ref. [27]. For additional details, see Fig. 7.

The influence of the PSF enhancement at very low ($E_\gamma <$ 2 MeV) energies was tested. Our data are in striking disagreement to simulations using the $M1$ PSF, including a low-energy enhancement of the form proposed in Refs. [27,54]; see Fig. 11. Such enhancement produces excessive intensity of low-energy transitions, leading to unrealistic preference of high ($M \geqslant 5$) multiplicities.

We also tried to invoke a more "conservative" description of the ^{152,4}Sm$(p,d\gamma)$ data [27]—the low-energy enhancement was replaced by a low-lying Lorentzian resonance similar to the method in Ref. [67]. The parameters of this resonance were adjusted to match the shape of the ^{152,4}Sm$(p,d\gamma)$ data and scaled down to the data from the ^{3}He-induced reactions [20,21]. For the simulations in Fig. 11, we used 0.55 MeV, 0.45 MeV, and 0.20 mb for the energy, width and maximum cross section of this low-energy resonance, respectively. In general, any suppression of the low-energy enhancement with respect to the form proposed in Ref. [27] leads to a relative suppression of the low-energy transitions and lowers the differences from the mean experimental MSC spectra, as can be seen in Fig. 11. However, even simulations with this restricted low-energy enhancement do not match the experiment and still display a strong, unrealistic preference of high ($M \geqslant 5$) multiplicities.

This kind of disagreement is consistently observed also in combinations with other standard $E1$ PSF and LD models. Further, we note that simulations with a part or even all of the low-energy enhancement strength moved to the $E1$ PSF give similarly unacceptable results.

V. COMPARISON WITH OTHER DATA

A. Available data

Relevant experimental information about the PSFs in the region of the SM in well-deformed even-even rare-earth nuclei comes from several sources. The PSFs were obtained from analyses of (n,γ) reactions, specifically the MSC and TSC measurements of ^{156,158}Gd [23,24,26]. Data on mixed dipole, $S^{(E1)} + S^{(M1)}$, PSFs came from measurements of the ^{3}He-induced reactions by the Oslo group for ^{160,162,164}Dy [19–21]. The ground-state transitions were studied in NRF experiments for all stable even-even rare-earth nuclei including ^{162,164}Dy [11,12]. In addition, the total radiation widths of s-wave neutron resonances are available for all stable nuclei [32,38].

B. Total radiation width

The total radiation width of s-wave neutron resonances, Γ_γ, is in general the only quantity simulated with the DICEBOX code that depends on the absolute values of the PSFs. As such, it can be used to further restrict the acceptability of the model combinations found from the comparison of simulated MSC spectra with their experimental counterparts.

Although the majority of LD and $E1$ PSF models can be rejected just from the comparison of mean experimental and simulated MSC spectra, the resulting Γ_γ can provide additional support for such conclusions. The simulations using the CT LD model give a Γ_γ comparable with the experimental value only when the SLO model of $E1$ PSF is used. However, for this combination of LD and $E1$ PSF models, we were unable to adjust the $M1$ PSF to reproduce the mean experimental MSC spectra.

The Γ_γ for the model combinations which provide acceptable descriptions of mean experimental MSC spectra are listed in Table II. The comparison to experimental values indicates that the combination with the KMF model is likely rejected, at least for ^{164}Dy. In addition, there is a value of the MGLO parameter k that perfectly reproduces the experimental Γ_γ for each isotope. However, the required values of the parameter are different: slightly higher than $k = 2$ for ^{162}Dy while just below $k = 4$ for ^{164}Dy. Suitability of the MGLO model is achieved by a change of the k parameter with the mass number.

In the rest of the discussion, we will consider only the PSF models reproducing both mean experimental MSC spectra and Γ_γ. Assuming the MGLO model for $E1$ PSF, this restriction means $k \approx 2$ and $\sigma_{\rm SM} = 0.2$–0.3 mb and $S_{\rm SP}^{(M1)} = 2$–4×10^{-9} MeV^{-3} for ^{162}Dy and value of $k \approx 4$ and $\sigma_{\rm SM} = 0.5$–0.6 mb

TABLE II. Total radiation width of s-wave neutron resonances. The simulations are labeled with the used LD and $E1$ PSF model; the $M1$ PSF was adjusted as described in Sec. IV C. The experimental values are taken from Refs. [32,38].

Γ_γ (meV)	^{162}Dy		^{164}Dy	
PSF \ LD	BSFG	CT	BSFG	CT
KMF	92(2)	43(1)	69(2)	38(1)
MGLO ($k = 2$)	105(2)	51(2)	80(2)	45(1)
MGLO ($k = 4$)	176(3)	85(1)	114(3)	61(2)
Experiment	107(3)		105(8)	

for ^{164}Dy; no SP model was allowed for ^{164}Dy (see Sec. IV C). The SM parameters allowing simultaneous reproduction of both discussed observables are summarized in Table III.

C. Scissors mode

1. Comparison with NRF data

To compare our results with the summed $M1$ strength as determined in NRF experiments, we have integrated all $M1$ strength in the energy range 2.7–3.7 MeV.

The value obtained for ^{162}Dy using the composite model of $M1$ PSF $S^{(M1)} = S^{(M1)}_{\rm SM} + S^{(M1)}_{\rm SF} + S^{(M1)}_{\rm SP}$ is 2.4(4) μ^2_N, in excellent agreement with the summed $M1$ strength of 2.49(13) μ^2_N [11]. We should note here that in our model the SM contributes roughly 60% of the strength. The tail of SF resonances and especially the SP strength are responsible for the rest of this summed $M1$ strength. The centroid value of 2.956(4) MeV from NRF data [11] agrees with our findings.

Our integrated M1 strength for ^{164}Dy $\sum B(M1) =$ 3.8(7) μ^2_N is compatible with the strength 3.18(15) μ^2_N observed in the NRF experiment [12]. The centroid of the $M1$ strength from the NRF data was determined to be 3.143(2) MeV, in contrast to our result of $E_{\rm SM} = 2.8$–3.0 MeV. However, these numbers are not directly comparable because the centroid from NRF is distorted from the $E_{\rm SM}$ as all observed $M1$ transitions in the restricted energy range $E_\gamma = 2.7$–3.7 MeV were used in the NRF calculation. Thus, the agreement of the centroid position in ^{162}Dy might be coincidental.

2. Comparison with Oslo results

The SM parameters from the ^{3}He-induced reaction in ^{162}Dy are $E_{\rm SM} = 2.6$–2.7 MeV, $\Gamma_{\rm SM} = 0.8$–1.3 MeV, and $\sigma_{\rm SM} = 0.3$–0.4 mb [20]. Our simulations require higher $E_{\rm SM} = 2.8$–3.0 MeV with $\Gamma_{\rm SM} = 1.0$–1.4 MeV and $\sigma_{\rm SM} =$ 0.2–0.3 mb. The parameters from these two sources are not fully compatible, especially for the $E_{\rm SM}$.

In the case of ^{164}Dy, the authors of Ref. [21] determined the position $E_{\rm SM} = 2.81(6)$ MeV, which is in agreement with our result. Their result of $\sigma_{\rm SM} = 0.53(6)$ mb also nicely agrees with our accepted interval of $\sigma_{\rm SM} = 0.5$–0.6 mb. However, the value of $\Gamma_{\rm SM} = 0.80(12)$ MeV from Ref. [21] is slightly lower compared to our interval of $\Gamma_{\rm SM} = 1.0$–1.4 MeV.

Contrary to the restricted energy range used to compare all $M1$ strength with the NRF data, the total SM strength can be compared to the Oslo results. In ^{162}Dy, the total SM strength given by our best models $\sum B(SM) = 2.3$–4.3 μ^2_N is significantly lower than the strength of 6.8(8) μ^2_N corresponding to PSFs in Ref. [20]. For ^{164}Dy, our determined SM strength is $\sum B(SM) = 5.3$–7.5 μ^2_N, which is comparable to 5.4(10) μ^2_N from Ref. [21].

One should keep in mind that the comparison of the SM parameters is not as straightforward as it might seem. The parameters from Refs. [20,21] depend on the exact choice of the $E1$ PSF model. For instance, significant influence of the nuclear temperature T in the KMF-T model on the SM parameters was shown in Ref. [20]. Moreover, we have to assume a significant SP contribution in ^{162}Dy $S^{(M1)}_{\rm SP} =$ 2–4 $\times$ 10^{-9} MeV^{-3}. The possible contribution of $S^{(M1)}_{\rm SP}$ is not accounted for in Refs. [20,21].

TABLE III. The parameters of the scissors mode reproducing both the mean experimental MSC spectra and the total radiation width as deduced in our analysis.

Isotope	$E_{\rm SM}$ (MeV)	$\Gamma_{\rm SM}$ (MeV)	$\sum B(SM)$ (μ^2_N)
^{162}Dy	2.8–3.0	1.0–1.4	2.3–4.3
^{164}Dy	2.8–3.0	1.0–1.4	5.3–7.5

3. Comparison with Gd MSC results

The allowed intervals of SM and SP parameters deduced from analyses of MSC spectra in even-even Gd isotopes [23,24] are fully compatible with our ^{162}Dy results. Contrary to this, the total SM strength in ^{164}Dy from our analysis is 2–3$\times$ higher when compared to ^{156,158}Gd and ^{162}Dy. Moreover, the highest allowed SP strength in ^{164}Dy is at least 2–3$\times$ lower than $S^{(M1)}_{\rm SP}$ in ^{156,8}Gd and ^{162}Dy, being compatible in these three nuclei.

VI. FLUCTUATION PROPERTIES OF MSC SPECTRA

The experimental MSC spectra were obtained for tens of resonances of both spins for each nucleus. This number of resonances should allow us, contrary to our previous works [23,24], to draw some conclusions about observed fluctuations of MSC intensities.

A. Extended simulations of MSC intensities

As mentioned in Sec. III A, we have extended the DICEBOX algorithm by introducing nuclear subrealizations to access different sources of fluctuations. For a couple of combinations of PSF and LD models, we have performed extended simulations with $L = 50$ nuclear subrealizations within each of $N = 50$ nuclear realizations. We chose model combinations providing a satisfactory description of the mean experimental MSC spectra and total radiation width as given in Secs. IV and V B, including the model combinations presented in Figs. 7 and 8.

It turns out that for the MSC intensity $I_{\lambda\nu}$ the counting uncertainty $\Delta^{\rm MC}_{\lambda\nu}$ reached in our simulations is low enough that it does not have any influence on computed measures of

distributions introduced in Sec. III A. This statement is based on the fact that for any given NR ν' the realization mean $a_{\nu'}$ and the fluctuation of subrealizations $\sigma_{\nu'}$ obtained from a maximum likelihood fit of the set $\{I_{\lambda\nu'}, \Delta^{\mathrm{MC}}_{\lambda\nu'}\}^{L}_{\lambda=1}$ are virtually equal to the average and standard deviation of the set $\{I_{\lambda\nu'}\}^{L}_{\lambda=1}$, respectively.

When using the maximum likelihood fit as introduced in Eq. (1), it was assumed that the MSC intensities are normally distributed. To justify this assumption, we tested whether the sets of simulated MSC intensities $\{I_{\lambda\nu'}\}^{L}_{\lambda=1}$ for all NRs $\nu' = 1, \ldots, N$ are normally distributed with means $a_{\nu'}$ and a common variance σ^2 using the properly adjusted testing statistics proposed by Zhang in Ref. [68]. Thanks to a superior power of used testing statistics, minor deviations from the normal distribution were detected. However, we can claim that in energy bins between E_{crit} and $S_n - E_{\mathrm{crit}}$ in $M = 2$ spectra and in all bins with the MSC intensity significantly higher than zero in $M \geqslant 3$ spectra the distribution of MSC intensities is so close to the normal distribution that the form of the likelihood function as defined in Eq. (1) is a well-justified approximation.

We checked several other features of simulations. We tested whether the sets $\{\sigma^2_\nu\}^{N}_{\nu=1}$ display a ν dependence throughout energy bins, i.e., whether $\sigma_{\nu'}$ is systematically lower or higher than the average σ throughout different energy bins for a fixed realization ν'. For all of the tested PSF and LD model combinations, we observe no ν dependence of σ^2_ν between E_{crit} and $S_n - E_{\mathrm{crit}}$ in $M = 2$ spectra and in all bins with MSC intensity significantly higher than zero in multiplicities $M \geqslant 3$. In addition to that, the distribution of the set $\{\sigma_\nu\}^{N}_{\nu=1}$ is rather narrow with 90% falling into $\sigma \pm 20\%$ interval in all these energy bins. As a result, it seems appropriate to use the value of σ instead of the distribution of σ_ν when comparing with experimental fluctuations.

Moreover, we have not observed any correlation between fluctuations due to NRs and fluctuations due to nuclear subrealizations; i.e., the fluctuation of means, Σ, and the average fluctuation over subrealizations within realizations, σ, are statistically independent. From these findings, it follows that Σ, as the standard deviation of the set $\{a_\nu\}^{N}_{\nu=1}$, and σ can be extracted separately from our extended simulations.

For all tested model combinations, the fluctuation of means Σ was found to be about an order of magnitude lower than σ for almost all energy bins; see Figs. 12 and 13. The only exceptions are bins around $E_\gamma = 2$ MeV, where Σ reaches up to 50% and 80% of σ for ^{162}Dy and ^{164}Dy respectively; the symmetry of $M = 2$ MSC spectra around the midpoint leads to the same effect also at $E_\gamma = S_n - 2$ MeV. These energies correspond to cascades through levels at excitation energy of about 2 MeV, i.e., just above E_{crit} where the LD is relatively low. The uncertainty in the level scheme at these energies is expected to lead to significant fluctuations of predicted realization means a_ν, i.e., to a high value of Σ.

Low values of Σ (compared to σ) can be used as a justification of the assumption, used in the all our previous works, that the concept of NRs serves as a reasonable tool to overcome the inability to experimentally retrieve the level properties above E_{crit} without hindering the estimation of the mean MSC intensities and their fluctuations. Assuming that the fluctuations are well described in our simulations, we

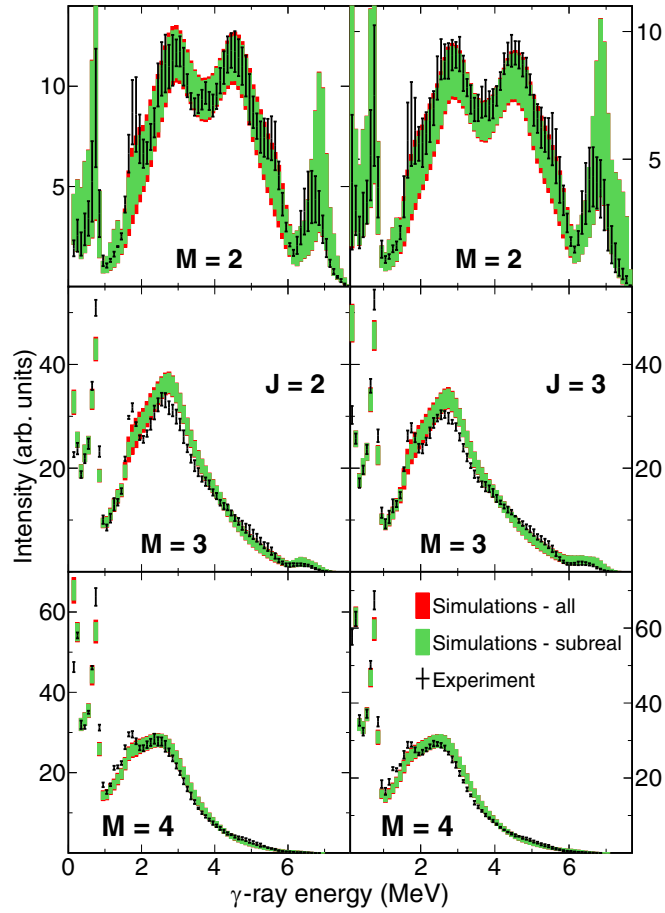

FIG. 12. Comparison of MSC intensities and their fluctuations from experiment and extended simulations for ^{164}Dy. Black symbols indicate $I_{\mathrm{exp}} \pm \sigma_{\mathrm{exp}}$ obtained from the maximum likelihood fit as described in Sec. II B. The green band corresponds to $a \pm \sigma$ and the red band to $a \pm \sqrt{\sigma^2 + \Sigma^2}$ as deduced from extended simulations with the BSFG LD model, MGLO $E1$ PSF model with $k = 4$ and the composite $M1$ PSF model with SM parameters $E_{\mathrm{SM}} = 3.0$ MeV, $\Gamma_{\mathrm{SM}} = 1.2$ MeV, and $\sigma_{\mathrm{SM}} = 0.6$ mb. The left and right columns show spectra for $J = 2$ and 3 resonances, respectively. The multiplicity M is indicated.

should not only require the mean experimental MSC intensity to coincide with the average coming from simulations when performing a search for appropriate PSF and LD models as presented in Sec. IV. At the same time, the estimate of fluctuations from simulations, represented by gray bands in Figs. 7–11, should be comparable to the fluctuations of experimental MSC intensities, depicted as red error bars in Figs. 7–11. However, we should stress that our findings about the contribution of different sources of fluctuations in simulations are not necessarily universal for all nuclei and different behavior could be encountered for nuclei in different mass regions.

B. Comparison of experimental and simulated fluctuations

The fluctuations of experimental MSC intensities, σ_{exp}, of ^{164}Dy were found for both resonance spins to be on average lower by ≈30% than σ from simulations in bins between E_{crit} and $S_n - E_{\mathrm{crit}}$ in $M = 2$ spectra and in all

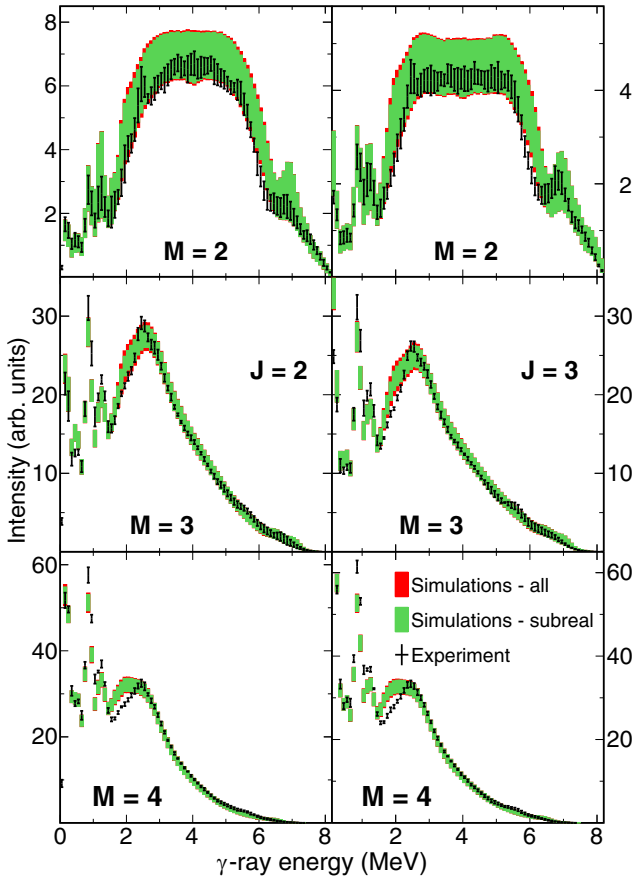

FIG. 13. The same as in Fig. 12 but for ^{162}Dy. In this case, the BSFG LD model, KMF $E1$ PSF model, and the composite $M1$ PSF model with $S_{\rm SP}^{(M1)} = 3 \times 10^{-9}$ MeV^{-3} and SM parameters $E_{\rm SM} = 2.8$ MeV, $\Gamma_{\rm SM} = 1.1$ MeV, and $\sigma_{\rm SM} = 0.2$ mb were used.

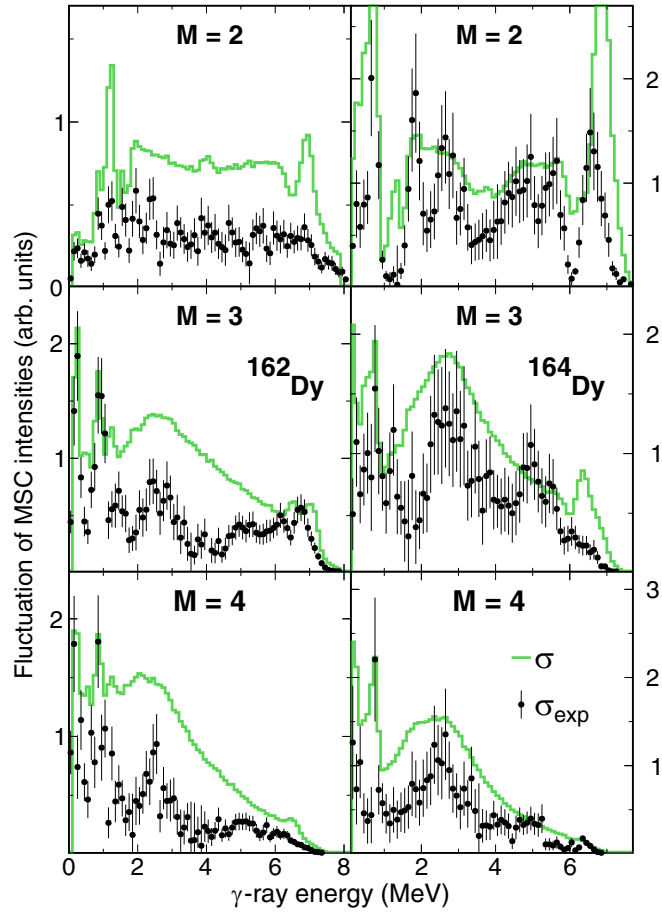

FIG. 14. Comparison of fluctuations of experimental MSC intensities $\sigma_{\rm exp}$ (black dots) with the average fluctuation over subrealizations within realizations σ (green line) for resonances with $J = 2$ in ^{162}Dy (left) and ^{164}Dy (right). The absolute values of experimental and simulated fluctuations presented in Figs. 12 and 13 as black error bars and green bands, respectively, are shown in this figure. The units on vertical axis correspond to units in Figs. 12 and 13. The uncertainty of $\sigma_{\rm exp}$ (error bar on the black point) was deduced from the maximum likelihood fit to experimental data as described in Sec. II B.

bins with MSC intensity significantly higher than zero in multiplicities $M \geqslant 3$; see Figs. 12 and 14. In reality, as evident from Fig. 14, the σ_{exp} exhibits significant oscillations among different energy regions of MSC spectra. Considering also the relatively high uncertainties of σ_{exp} it seems very difficult to make any definite conclusions about the agreement of experimental and simulated fluctuations in this nucleus.

The situation for ^{162}Dy was found to be very different, albeit consistent for both resonance spins. Values of $\sigma_{\rm exp}$ reach on average only 40% of σ values in the relevant energy range; see Figs. 13 and 14. This result was obtained for both tested model combinations, i.e., using KMF and MGLO ($k = 2$) models, as could be expected when using similar $E1$ PSF models.

The observed differences between σ and $\sigma_{\rm exp}$ (see Fig. 14) point to an inadequate description of fluctuations of primary transitions in our grand simulations with the LD and PSF models specified in Figs. 12 and 13.

This conclusion does not necessarily imply invalidity of the PT fluctuations. First, tested model combinations do not reproduce experimental spectra perfectly (see Figs. 12 and 13) and we expect that simulated fluctuations do depend on the adopted model combination. Moreover, in our trial and error search, we have restricted ourselves to standard models. Specifically, the chosen LD model displays smooth energy and spin dependence with no parity asymmetry. It is likely there are model combinations with more complicated LD behavior that would provide acceptable description of mean experimental MSC spectra while significantly changing the predicted fluctuations of MSC intensities σ. A higher number of levels at certain energy involved in the decay is expected to suppress the simulated fluctuations σ, i.e., the width of the green bands in Figs. 12 and 13.

Furthermore, the decay is described within the statistical model as implemented in the DICEBOX code [33]. This approach relies on a number of assumptions. Among others, it is assumed that pairs of partial radiation widths $\Gamma_{i\gamma f}$ and $\Gamma_{i\gamma f'}$ with $f \neq f'$ are not correlated and that the individual widths $\Gamma_{i\gamma f}$ of all states above $E_{\rm crit}$ fluctuate according to the PT distribution. While these assumptions are well justified for highly excited states such as neutron resonances, there might be additional effects at energies just above $E_{\rm crit}$. For instance, as we are dealing with a well-deformed nucleus one might

think about some influence of the quantum number K, which is not accounted for in the simulations.

Naturally, a question arises as to whether the results on LD and PSF models in Sec. IV would be altered by an universally different description of the fluctuations. Our initial tests with fluctuations according to both narrower and wider distributions of intensities show that influence of the distribution on the LD and PSF model selection is negligible.

VII. SUMMARY

A measurement of γ-ray spectra from s-wave neutron resonances in the ^{161,163}Dy(n,γ) reactions was performed with isotopically enriched targets at the DANCE detector array at the LANSCE spallation neutron source. The multistep cascades spectra for different multiplicities from tens of neutron resonances with different spins were used to test the validity of various PSF and LD models. A large number of measured resonances allowed the first meaningful analysis of observed fluctuations of MSC intensities.

Based on the comparison of experimental and simulated MSC spectra, we can make the following conclusions about the LD and PSF models: The energy dependence of the nuclear level density is well described with the BSFG model, while the dependence predicted by the CT model is highly improbable.

The allowed $E1$ PSF at energies below about 7 MeV has a relatively weak energy dependence similar to the model of Kadmenskii *et al.* [40] or the MGLO model [25]. If the total radiation width of neutron resonances is taken into account, the best description of the $E1$ PSF is given by the MGLO model. However, the parameter k of the MGLO model reaches different values in the two studied isotopes. Models of the $E1$ PSF with a steep γ-ray energy dependence (similar to a Lorentzian shape) at energies $E_\gamma \lesssim 5$–6 MeV are not acceptable.

The scissors mode, a resonance in the $M1$ PSF just below 3 MeV, was found essential when describing radiative decay of neutron resonances in ^{162,164}Dy isotopes. The scissors mode influences transitions at least up to the neutron separation energy. Within the sensitivity of our data, we gather that the resonance parameters are very stable with increasing excitation energy—the scissors mode seems to follow the Brink hypothesis. The parameters of the SM reproducing mean experimental MSC spectra and total radiation width are listed in Table III for both isotopes.

The $M1$ strength below about 4 MeV is consistent with the NRF data [11,12] while some deviations are found if our results are compared to Oslo data in corresponding isotopes [20,21]. Deduced $M1$ parameters for ^{162}Dy are fully consistent with those obtained from the analysis of MSC spectra for well deformed even-even Gd isotopes [23,24]. However, complete agreement with Gd parameters is not achieved for ^{164}Dy as the required $M1$ strength is 2–3$\times$ higher in this nucleus compared to ^{162}Dy.

An overall reasonable reproduction of the mean experimental MSC intensities for both spins of capturing states in both nuclei indicates that the standard description of γ decay within the statistical model and the concept of PSFs is suitable for deformed rare-earth nuclei.

The size of fluctuations of experimental MSC intensities among different neutron resonances is significantly smaller than the simulated one in ^{162}Dy for all relevant γ-ray energies. In ^{164}Dy, the size of experimental fluctuations is on average lower than the simulated one but the behavior is more complicated with evident γ-ray energy dependence. This observation may point to invalidity of the Porter-Thomas distribution assumed for fluctuations of individual transition intensities, but there are other possible explanations of the observed disagreement. In any case, we would be very cautious in making definite conclusions as the difference in results for the two nuclei is rather puzzling and further study of fluctuation properties is required.

ACKNOWLEDGMENTS

Two of us (S.V. and M.K.) would like to express our deepest gratitude to F. Bečvář for his idea to extend the DICEBOX simulations by introducing the nuclear subrealizations and for hours of discussion and encouragement during preparation of this article. This work was supported in part by the U.S. Department of Energy Grants No. DE-NA0001784 and No. DE-FG02-97-ER41042. This work benefited from the use of the LANSCE accelerator and was performed under the auspices of the U.S. Department of Energy at Los Alamos National Laboratory by the Los Alamos National Security, LLC, under Contract No. DE-AC52-06NA25396. It was also supported by Grant No. P203-13-07117S of the Czech Science Foundation and by the International Atomic Energy Agency project IAEA CRP F41032.

[1] G. J. Mathews and R. A. Ward, Rep. Prog. Phys. **48**, 1371 (1985).
[2] C. Sneden, J. J. Cowan, and R. Gallino, Annu. Rev. Astron. Astrophys. **46**, 241 (2008).
[3] Report of the Nuclear Physics and Related Computational Science R&D for Advanced Fuel Cycles Workshop (Bethesda, Maryland, 2006), http://www.osti.gov/scitech/servlets/purl/1298979.
[4] M. Heil, R. Reifarth, M. M. Fowler, R. C. Haight, F. Käppeler, R. S. Rundberg, E. H. Seabury, J. L. Ullmann, and K. Wisshak, Nucl. Instrum. Methods A **459**, 229 (2001).
[5] R. Reifarth, T. A. Bredeweg, A. Alpizar-Vicente, J. C. Browne, E.-I. Esch, U. Greife, R. C. Haight, R. Hatarik, A. Kronenberg, J. M. O'Donnell *et al.*, Nucl. Instrum. Methods A **531**, 530 (2004).
[6] R. R. Hilton, in *Proceedings of International Conference on Selected Topics in Nuclear Structure, Dubna, USSR, 1976*, edited by V. G. Soloviev (JINR, Dubna, 1976).
[7] N. Lo Iudice and F. Palumbo, Phys. Rev. Lett. **41**, 1532 (1978).
[8] F. Iachello, Nucl. Phys. A **358**, 89c (1981).
[9] D. Bohle, A. Richter, W. Steffen, A. E. L. Dieperink, N. Lo Iudice, F. Palumbo, and O. Scholten, Phys. Lett. B **137**, 27 (1984).
[10] C. Wesselborg, P. Von Brentano, K. O. Zell, R. D. Heil, H. H. Pitz, U. E. P. Berg, U. Kneissl, S. Lindenstruth, U. Seemann, and R. Stock, Phys. Lett. B **207**, 22 (1988).

[11] H. Friedrichs, B. Schlitt, J. Margraf, S. Lindenstruth, C. Wesselborg, R. D. Heil, H. H. Pitz, U. Kneissl, P. von Brentano, R. D. Herzberg *et al.*, Phys. Rev. C **45**, R892 (1992).

[12] J. Margraf, T. Eckert, M. Rittner, I. Bauske, O. Beck, U. Kneissl, H. Maser, H. H. Pitz, A. Schiller, P. von Brentano *et al.*, Phys. Rev. C **52**, 2429 (1995).

[13] U. Kneissl, H. H. Pitz, and A. Zilges, Prog. Part. Nucl. Phys. **37**, 349 (1996).

[14] U. Kneissl, N. Pietralla, and A. Zilges, J. Phys. G: Nucl. Part. Phys. **32**, R217 (2006).

[15] D. M. Brink, Ph.D. thesis, Oxford University, Oxford, UK, 1955 (unpublished).

[16] F. Bečvář, P. Cejnar, J. Honzátko, K. Konečný, I. Tomandl, and R. E. Chrien, Phys. Rev. C **52**, 1278 (1995).

[17] M. Krtička, F. Bečvář, J. Honzátko, I. Tomandl, M. Heil, F. Käppeler, R. Reifarth, F. Voss, and K. Wisshak, Phys. Rev. Lett. **92**, 172501 (2004).

[18] A. Schiller, A. Bjerve, M. Guttormsen, M. Hjorth-Jensen, F. Ingebretsen, E. Melby, S. Messelt, J. Rekstad, S. Siem, and S. W. Ødegård, Phys. Rev. C **63**, 021306(R) (2001).

[19] A. Voinov, M. Guttormsen, E. Melby, J. Rekstad, A. Schiller, and S. Siem, Phys. Rev. C **63**, 044313 (2001).

[20] M. Guttormsen, A. Bagheri, R. Chankova, J. Rekstad, S. Siem, A. Schiller, and A. Voinov, Phys. Rev. C **68**, 064306 (2003).

[21] H. T. Nyhus, S. Siem, M. Guttormsen, A. C. Larsen, A. Burger, N. U. H. Syed, G. M. Tveten, and A. Voinov, Phys. Rev. C **81**, 024325 (2010).

[22] H. T. Nyhus, S. Siem, M. Guttormsen, A. C. Larsen, A. Bürger, N. U. H. Syed, H. K. Toft, G. M. Tveten, and A. Voinov, Phys. Rev. C **85**, 014323 (2012).

[23] A. Chyzh, B. Baramsai, J. A. Becker, F. Bečvář, T. A. Bredeweg, A. Couture, D. Dashdorj, R. C. Haight, M. Jandel, J. Kroll *et al.*, Phys. Rev. C **84**, 014306 (2011).

[24] B. Baramsai, J. Kroll, G. E. Mitchell, U. Agvaanluvsan, F. Bečvář, T. A. Bredeweg, A. Chyzh, A. Couture, D. Dashdorj, R. C. Haight *et al.*, Phys. Rev. C **87**, 044609 (2013).

[25] J. Kroll, B. Baramsai, G. E. Mitchell, U. Agvaanluvsan, F. Becvar, T. A. Bredeweg, A. Chyzh, A. Couture, D. Dashdorj, R. C. Haight *et al.*, Phys. Rev. C **88**, 034317 (2013).

[26] S. Valenta, F. Bečvář, J. Kroll, M. Krtička, and I. Tomandl, Phys. Rev. C **92**, 064321 (2015).

[27] A. Simon, M. Guttormsen, A. C. Larsen, C. W. Beausang, P. Humby, J. T. Burke, R. J. Casperson, R. O. Hughes, T. J. Ross, J. M. Allmond *et al.*, Phys. Rev. C **93**, 034303 (2016).

[28] J. M. Wouters, A. A. Vicente, T. A. Bredeweg, E. Esch, R. C. Haight, R. Hatarik, J. M. O'Donnell, R. Reifarth, R. S. Rundberg, J. M. Schwantes *et al.*, IEEE Trans. Nucl. Sci. **53**, 880 (2006).

[29] M. Jandel, T. A. Bredeweg, A. Couture, M. M. Fowler, E. M. Bond, M. B. Chadwick, R. R. C. Clement, E.-I. Esch, J. M. O'Donnell, R. Reifarth *et al.*, Nucl. Instrum. Methods Phys. Res. B **261**, 1117 (2007).

[30] P. W. Lisowski, C. D. Bowman, G. J. Russell and S. A. Wender, Nucl. Sci. Eng. **106**, 208 (1990).

[31] F. Bečvář, P. E. Koehler, M. Krtička, G. E. Mitchell and J. L. Ullmann, Nucl. Instrum. Methods A **647**, 73 (2011).

[32] S. F. Mughabghab, *Atlas of Neutron Resonances* (Elsevier, Amsterdam, 2006).

[33] F. Bečvář, Nucl. Instrum. Methods A **417**, 434 (1998).

[34] C. W. Reich, Nucl. Data Sheets **108**, 1807 (2007).

[35] B. Singh, Nucl. Data Sheets **93**, 243 (2001).

[36] C. E. Porter and R. G. Thomas, Phys. Rev. **104**, 483 (1956).

[37] T. Kibédi, T. W. Burrows, M. B. Trzhaskovskaya, P. M. Davidson, and C. W. Nestor Jr., Nucl. Instrum. Methods A **589**, 202 (2008).

[38] R. Capote, M. Herman, P. Obložinský, P. G. Young, S. Goriely, T. Belgya, A. V. Ignatyuk, A. J. Koning, S. Hilaire, V. A. Plujko *et al.*, Nucl. Data Sheets **110**, 3107 (2009).

[39] S. S. Dietrich and B. L. Berman, At. Data Nucl. Data Tables **38**, 199 (1988).

[40] S. G. Kadmenskii, V. P. Markushev, and V. I. Furman, Sov. J. Nucl. Phys. **37**, 165 (1983).

[41] R. E. Chrien, in *Proceedings of the 5th International School on Neutron Physics, Alushta, USSR, 1987*, edited by B. B. Kolesova and V. R. Sarantseva, JINR Report No. D3, 4, 17-86-747 (JINR, Dubna, USSR, 1987).

[42] J. Kopecky, M. Uhl, and R. E. Chrien, Phys. Rev. C **47**, 312 (1993).

[43] S. Goriely, Phys. Lett. B **436**, 10 (1998).

[44] S. F. Mughabghab and C. L. Dunford, Phys. Lett. B **487**, 155 (2000).

[45] V. A. Plujko, O. M. Gorbachenko, E. P. Rovenskykh, and V. A. Zheltonozhskii, Nucl. Data Sheets **118**, 237 (2014).

[46] L. M. Bollinger and G. E. Thomas, Phys. Rev. C **2**, 1951 (1970).

[47] T. von Egidy and D. Bucurescu, Phys. Rev. C **72**, 044311 (2005); **73**, 049901(E) (2006).

[48] T. von Egidy and D. Bucurescu, Phys. Rev. C **80**, 054310 (2009).

[49] D. Savran, T. Aumann, and A. Zilges, Prog. Part. Nucl. Phys. **70**, 210 (2013).

[50] D. Frekers, H. J. Wörtche, A. Richter, R. Abegg, R. E. Azuma, A. Celler, C. Chan, T. E. Drake, R. Helmer, K. P. Jackson *et al.*, Phys. Lett. B **244**, 178 (1990).

[51] D. Bohle, G. Küchler, A. Richter, and W. Steffen, Phys. Lett. B **148**, 260 (1984).

[52] W. Ziegler, C. Rangacharyulu, A. Richter, and C. Spieler, Phys. Rev. Lett. **65**, 2515 (1990).

[53] N. Pietralla, P. von Brentano, R.-D. Herzberg, U. Kneissl, N. Lo Iudice, H. Maser, H. H. Pitz, and A. Zilges, Phys. Rev. C **58**, 184 (1998).

[54] R. Schwengner, S. Frauendorf, and A. C. Larsen, Phys. Rev. Lett. **111**, 232504 (2013).

[55] B. A. Brown and A. C. Larsen, Phys. Rev. Lett. **113**, 252502 (2014).

[56] R. Schwengner, S. Frauendorf, and B. A. Brown, Phys. Rev. Lett. **118**, 092502 (2017).

[57] K. Sieja, Phys. Rev. Lett. **119**, 052502 (2017).

[58] E. Litvinova and N. Belov, Phys. Rev. C **88**, 031302(R) (2013).

[59] T. Ericson, Adv. Phys. **9**, 425 (1960).

[60] Y. Alhassid, S. Liu, and H. Nakada, Phys. Rev. Lett. **99**, 162504 (2007).

[61] K. Kaneko and A. Schiller, Phys. Rev. C **75**, 044304 (2007).

[62] T. von Egidy and D. Bucurescu, Phys. Rev. C **78**, 051301(R) (2008).

[63] Y. Alhassid, L. Fang, and H. Nakada, Phys. Rev. Lett. **101**, 082501 (2008); Y. Alhassid (private communication).

[64] S. I. Al-Quraishi, S. M. Grimes, T. N. Massey, and D. A. Resler, Phys. Rev. C **67**, 015803 (2003).

[65] S. Goriely, S. Hilaire, and A. J. Koning, Phys. Rev. C **78**, 064307 (2008).

[66] A. J. Koning, S. Hilaire, and S. Goriely, Nucl. Phys. A **810**, 13 (2008).

[67] M. Krtička, F. Bečvář, I. Tomandl, G. Rusev, U. Agvaanluvsan, and G. E. Mitchell, Phys. Rev. C **77**, 054319 (2008).

[68] J. Zhang, J. R. Statist. Soc. B **64**, 281 (2002).